10/7/1989 (1)

SANDIA REPORT

SAND89—0079 • UC—253
Unlimited Release
Printed June 1989

PDC Bit Research at Sandia National Laboratories

John T. Finger, David A. Glowka

Prepared by
Sandia National Laboratories
Albuquerque, New Mexico 87185 and Livermore, California 94550
for the United States Department of Energy
under Contract DE-AC04-76DP00789

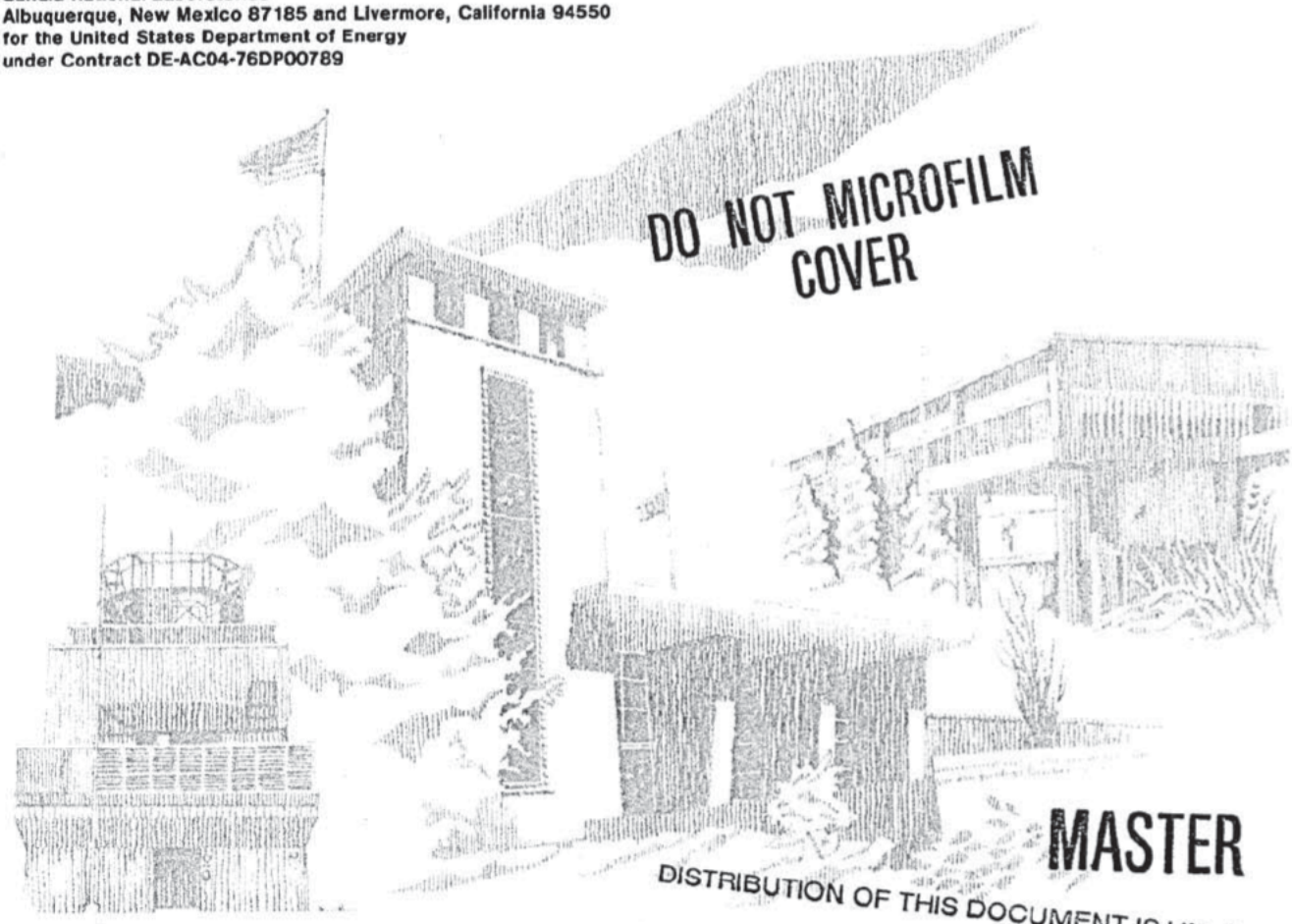

SF2900Q(8-81)

DISCLAIMER

DO NOT MICROFILM
THIS PAGE

Issued by Sandia National Laboratories, operated for the United States Department of Energy by Sandia Corporation.

Available to DOE and DOE contractors from
Office of Scientific and Technical Information
PO Box 62
Oak Ridge, TN 37831

Prices available from (615) 576-8401, FTS 626-8401

Available to the public from
National Technical Information Service
US Department of Commerce
5285 Port Royal Rd
Springfield, VA 22161

NTIS price codes
Printed copy: A05
Microfiche copy: A01

Distribution Category UC-253

SAND89-0079
Unlimited Distribution
Printed June 1989

SAND--89-0079

DE89 013885

PDC BIT RESEARCH AT SANDIA NATIONAL LABORATORIES

John T. Finger
David A. Glowka

Geothermal Research Division 6252
Sandia National Laboratories
Albuquerque, NM 87185

ABSTRACT

From the beginning of the geothermal development program, Sandia has performed and supported research into polycrystalline diamond compact (PDC) bits. These bits are attractive because they are intrinsically efficient in their cutting action (shearing, rather than crushing) and they have no moving parts (eliminating the problems of high-temperature lubricants, bearings, and seals.) This report is a summary description of the analytical and experimental work done by Sandia and our contractors. It describes analysis and laboratory tests of individual cutters and complete bits, as well as full-scale field tests of prototype and commercial bits. The report includes a bibliography of documents giving more detailed information on these topics.

This work was supported by the U. S. Department of Energy at Sandia National Laboratories under Contract DE-AC04-76DP00789.

TABLE OF CONTENTS

EXECUTIVE SUMMARY

This description of Sandia's work in PDC bit research is focused on the efforts of our staff and our contractors. By observing trends in industry, we have identified targets for our research and we have published the research results as widely as possible. It is difficult to assess the effect of this work on the drilling industry, however, so that topic is not addressed directly in this report.

The general strength of the PDC bit industry is shown by its increasing market share, in spite of higher PDC bit cost relative to roller-cone bits. This is primarily the result of design evolution that permits these inherently efficient bits to be used in a greater variety of formations. In some cases, highly site-specific, PDC bits have shown dramatic improvements in bit life and rate of penetration. The demonstrated saving of $100,000 to $200,000 in a single bit run makes it clear that this technology can have a major economic impact, but associating those savings with a particular piece of research or development is tenuous. It is safe to say, however, that our research has increased the interest, activity, and understanding in the field of PDC bit technology and thus has been a catalyst to that industry.

Our most important contributions have been analytic and catalytic. Our analysis has followed a reasonably coherent path from consideration of a single cutter moving through virgin rock to synthesis of a computer code for design and operation of a complete bit. We have worked with the bit industry at each step on this path and our efforts have stimulated them by reducing their risks of development and testing. The major elements in the program include the following:

Early research on the fundamental nature of the diamond/WC bond and the cutting process -- This work was done with GE on a contract basis.

Non-destructive testing of brazed cutter bonds -- Cutter detachments from the studs during field tests led to the development of an ultrasonic NDT technique for evaluating

brazed joints. This technique stimulated development of a better brazing method at General Electric.

Development of a diffusion bonding process for attachment of cutters to studs -- This was also an outgrowth of the braze-joint failures, and was a narrowly focused effort to solve that specific manufacturing problem.

Cutter placement design code -- A computer code that specified cutter layout on an arbitrary bit face was used by many bit manufacturers.

Full scale tests of complete bits -- Bits were tested in the laboratory to evaluate differences in their performances and lifetimes. These differences were significant and identified several areas of research. Bits were also field tested in cooperation with Unocal Geothermal and several bit manufacturers.

Bit hydraulics -- A test facility allowed direct observation of drilling-fluid flow patterns across the face of a bit; this was important for studying the effect of nozzle layout on cleaning and cooling. The test stand design was adopted by industry and used by bit manufacturers.

Modeling rock mechanics -- A finite-element model of the mechanical interaction between the rock and a cutter gave good qualitative representation of the cutting process, but numerical force values were often unrealistic because of rock's complexity as a medium.

Thermal modeling -- To analyze the frictional heating of the cutter by the rock was crucial, because cutter temperature and wear rate are closely correlated. The analytic results were verified by good agreement with experiments.

Single cutter tests -- Laboratory tests of single cutters, in many configurations, gave empirical values used in subsequent analysis and clarified aspects of the cutting process.

Water jets -- Extensive analytical and experimental investigation of high pressure water jets described their behavior and showed how they could be used for direct rock cutting by erosion and for augmentation of PDC shear cutting.

Bit design and operation code -- Much of the above work has been combined in a computer code that will aid in the design of a PDC bit or will generate an operating envelope for an existing bit. Copies of this code have been supplied to bit manufacturers.

The bit design code is the culmination of Sandia's PDC research. Promising areas for future effort include: verification of the design code with field data, modification of analyses with data from pressurized cutting, and evaluation of new cutter configurations.

Introduction -- POLYCRYSTALLINE DIAMOND COMPACT (PDC) BITS

The introduction of the man-made polycrystalline diamond cutting element, marketed by General Electric under the name STRATAPAX, heralded a revolution in the drill bit industry. Cutting elements, or compacts, of sintered diamond grains could be made in large, convenient sizes and did not have the cleavage planes of natural diamonds. The drag bit, a concept which had lain almost dormant for many years, was revived. New designs were fitted with the improved cutters, and they were run in almost every conceivable formation. As with most new technologies in high-risk enterprises, there were heartening successes and spectacular failures, but two features made these bits extremely attractive for geothermal use. Monolithic construction meant no moving parts, thus eliminating the problems of high-temperature bearings, seals, and lubricants; and a fundamentally different way of removing the rock (shearing, not crushing) drastically improved rate of penetration. These features, coupled with successful field experiences such as the Sandia-sponsored drilling with Unocal in the Valles Caldera, were a strong incentive to the development of PDC bits for the geothermal industry.

PDC bits also became very popular in the oil patch -- in the early 1980's more than 20 companies were manufacturing them in a variety of configurations (fig I.1). The bits had some success in geothermal drilling where the formations were sedimentary, but most of our effort has been directed toward making them effective in the hard, fractured rocks so characteristic of hot reservoirs. Those efforts are described in this report.

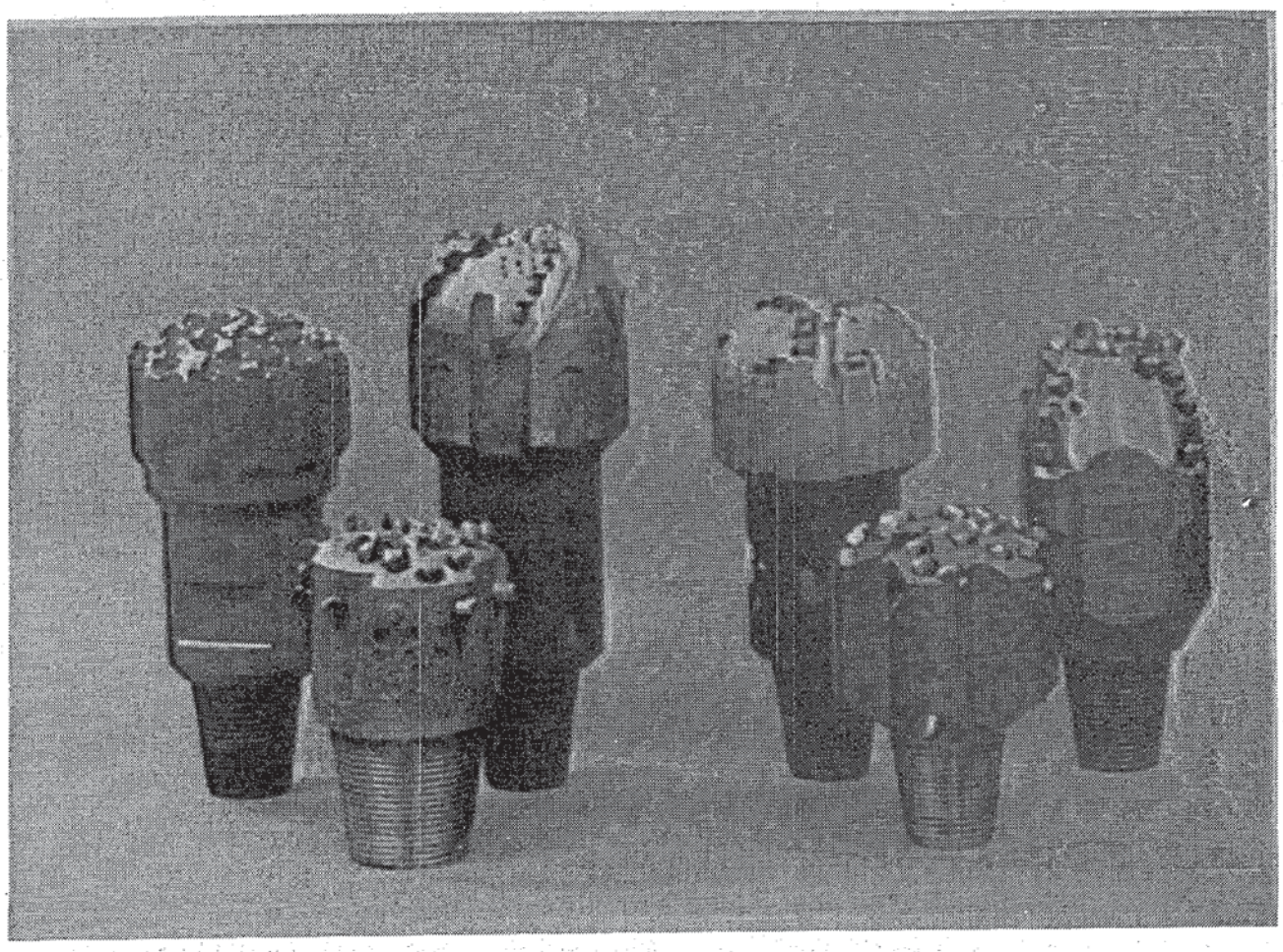

Figure I.1 -- Assortment of PDC bits showing variations in bit profile, cutter density, and cutter placement.

1 -- DIFFUSION BONDING FOR PDC CUTTERS

The search for a better method of mounting PDC cutters was stimulated by early field and laboratory tests on complete bits (section 2) in which one of the most common failures was the detachment of the PDC cutting element from the tungsten carbide mounting stud (fig 1.1). This was generally a catastrophic failure for two reasons: the detached compact became a very aggressive piece of junk in the bottom of the hole, and the unprotected stud quickly wore down far enough to quit cutting rock, thus stopping the bit's advance.

Failure analysis of the test bits and examination of new bits which had never been used for drilling (Ref. 1) showed that the brazed attachment of the compact's tungsten carbide substrate to the stud was often defective in at least three ways:

Hot shortness developed during brazing (Hot shortness means that liquid films form along grain boundaries and there is an instantaneous loss of strength -- this can also happen during drilling with inadequate cooling. Even if the film re-solidifies there will be cracks at the boundaries).

Areas of nonbonding caused by oxidation of the braze during brazing

Nonbonding caused by contamination of the braze before brazing.

These problems were aggravated by the inability of conventional ultrasonic inspection to detect them.

In an effort to solve the brazing problem by eliminating it, Sandia launched an investigation and development of diffusion bonding for cutter attachment (Refs 2,3). Diffusion bonding is a high pressure, high temperature, solid phase welding technique. If two very flat (within 10 Angstroms) surfaces are brought together under high pressure, a sufficiently high temperature will cause diffusion of the surface impurities and base materials -- thus welding the two materials together.

After producing several hundred diffusion bonded cutter assemblies, Sandia had developed a process recipe which is described

in detail in Reference 4. The development work also included an evaluation of other bonding techniques (e.g., metal foil in the bond line) and of alternate stud materials (two nickel alloys - Hastelloy B and Monel K500; five steels - ASTM A710, 4340, 4820, 9-4-20, and Maraging 250).

If non-tungsten-carbide studs are desirable, then two of the steels - 4820 and Maraging 250 - and the Monel K500 appear to be good candidates. Studs made from the alternate materials are cheaper, tougher, and easier to remove from a bit body than those made from tungsten carbide. The stiffness of carbide studs gives better support to the diamond compacts and their hardness reduces friction wear.

The addition of the nickel and titanium foils to the bond line modestly reduces the maximum shear strength compared to bare surfaces, but increases the bond toughness. All of the bond strengths in the tested materials (50,000 -70,000 psi) are adequate for drilling applications.

The diffusion bonding process is proven technology. The original motivation of eliminating brazing problems is less important now, because improved brazes are used by bit manufacturers and they provide, at least at room temperature, strengths equal to the diffusion bonded joints. It is not clear (no published data) how the strengths of brazed and diffusion bonded PDC cutter assemblies compare at high temperatures. Although brazing seems to work well in current geothermal applications, new and more extreme environments might once again generate a need for diffusion bonding.

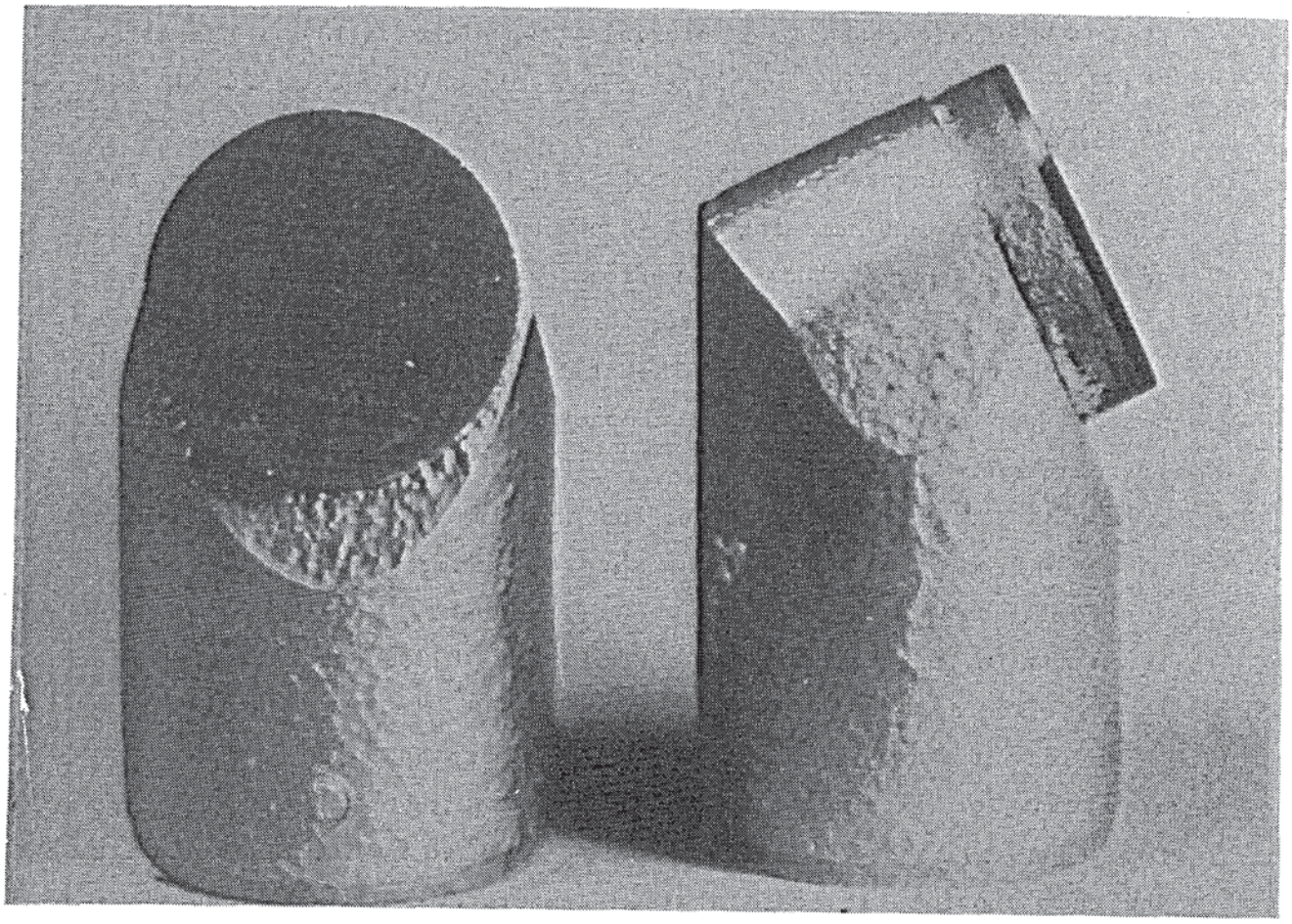

Figure 1.1 -- Front and side views of a single PDC cutter. The diamond layer is approximately 0.025" thick and 0.50" in diameter.

2 -- FULL SCALE BIT TESTS

Early in the geothermal technology development program we tested many PDC bits in the field and in the laboratory (Ref 5-8). The purpose of these tests was usually either to decide whether a particular formation could be drilled with a PDC bit or to compare the performance of different bit designs operating under identical conditions. Bit performance ranged from gratifying to disastrous. Drilling parameters, such as torque, rate of penetration, and failure mode were quite different among the various bits.

Samples of the kind of data collected in the laboratory tests appear in figures 2.1 - 2.3 and the postmortem analyses of the field test bits are in the references cited above. Certain gross conclusions about the suitability of a given bit in a given rock under given drilling conditions were possible, but it was very difficult to extrapolate these into any kind of generality. The design variables of the bits were so numerous, and in some cases so subtle, that inferences about cause/effect relationships were frequently tenuous. In spite of the unsystematic approach, we repeatedly identified several problems with using PDC bits in hard, hot formations.

The cutter bonding failure described in section 1 is obviously crucial -- it destroyed several bits but it is apparently now under control.

Gage cutters were particularly vulnerable and we have learned that this area must be very carefully designed, frequently with redundant cutters.

Cutter temperature is critical. We give a more complete and accurate statement of this in sections 7 and 9, but the basic notion is clear from the full scale tests. The value of using mud as drilling fluid instead of air is related to this, and is described later in detail.

The performance and, especially, lifetime of identical bits can vary enormously in different rocks. Some rocks may simply be too hard to drill with PDC bits.

Not all the results were bad. A 12-1/4 inch PDC bit used in the relatively soft sedimentary formation of the Imperial

Valley drilled twice as fast with half the wear of a roller cone bit used in the same interval.

We have much better insight now into these effects, and we have analytic, quantitative descriptions of each of these behaviors. Full scale bit testing is hard to control and is seriously expensive, but it will never be eliminated from the development of new bits. That's as it should be, but we hope that a more orderly bit design procedure will give industry a headstart on putting the right bit in the hole and will make the full scale test a proof of concept, not a design iteration.

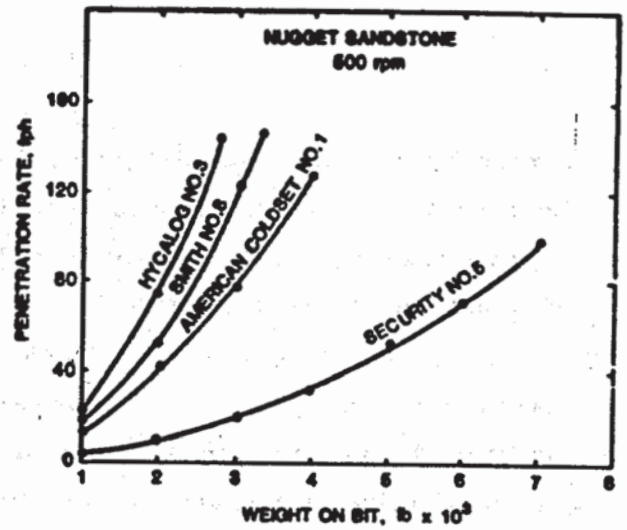

Figure 2.1 -- Performance of various bits at 500 rpm in Nugget Sandstone

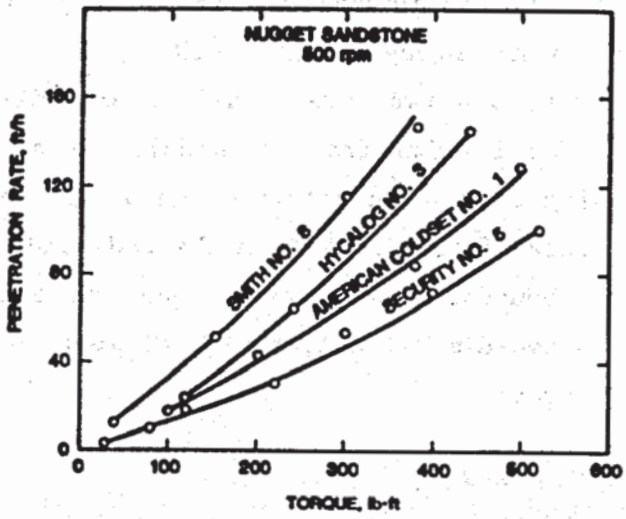

Figure 2.2 -- Torque characteristics of various bits at 500 rpm in Nugget Sandstone

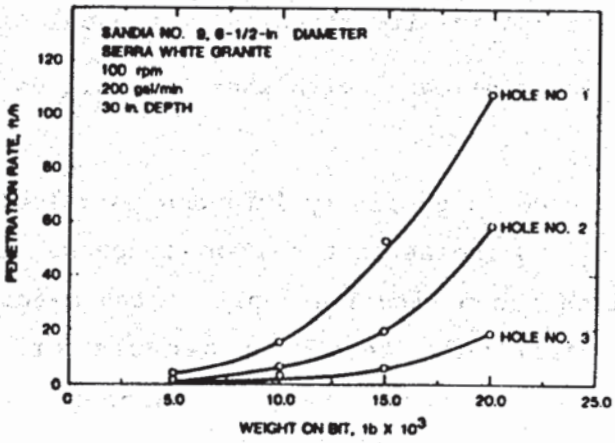

Figure 2.3 -- Performance of Sandia-designed bit at 100 rpm in Sierra White granite

PDC bits remove rock by a shearing action, much like a machine tool, which places the rock in tension. Because rock is far weaker in tension than in compression, this is inherently efficient compared to the crushing action of a roller-cone bit or the grinding effect of a diamond bit, which cause the rock to fail in compression. Actually designing a bit, however, is quite complicated. The individual cutters can vary in diameter, rake angle, clearance angle, side rake, and depth of cut while the whole bit will reflect choices in number of cutters, cutter placement, and bit profile. Our intent, therefore, was to ease this design process by gaining a better understanding of how cutters form chips. The analytic description of this is grounded in the simplest case, that of a single cutter moving through virgin rock.

Early modeling used a two-dimensional, finite-difference code (TOODY) that included a biaxial fracture model. These calculations were useful in showing the cyclic nature of chip formation, but they were hindered by a lack of flexibility in the code and its inability to accept realistic boundary conditions. When we transferred the model to HONDO II, a two-dimensional, finite-element code, we gained the following advantages:

Lower computing costs

Ability to specify boundary conditions on small samples (large sample sizes aren't needed)

Ability to include in-situ stresses in the calculations

An improved material model with shear as well as tensile failure.

The HONDO II code is generally intended to calculate the large deformation elastic and inelastic transient response of axisymmetric solids. It requires a constitutive model of the material, and this is particularly difficult for rock because of its abundant anisotropies and microflaws. Many researchers have proposed constitutive models for geologic materials; none of them is

complete, but a satisfactory start can be made if the following features are present: linear behavior in the elastic range, brittle cracking in tension, a pressure-dependent failure criterion in compression, and a post-failure material description.

Two constitutive relations with different compression failure criteria were used in the drag-bit modeling. One is a Coulomb criterion in which a closed crack can carry a shear load defined by the Coulomb friction model and the stress normal to the crack. The other is an elastic-plastic model which assumes that plastic flow occurs and that a closed crack heals to its original strength. These relations effectively provide upper and lower bounds on the post-failure strength of the material. If the rock is under no confining pressure, there will be little stress normal to a crack and it will carry little shear load in the Coulomb model, while high confining pressures will raise the Coulomb shear load near that of the elastic-plastic model. Figure 3.1 shows this effect.

Once the details of the theoretical model were fixed, it was necessary to have numerical values for the rock properties used in the calculations. To get these, we took samples of Berea sandstone and contracted with an outside laboratory for uniaxial and triaxial compression tests and Brazilian tensile tests. A summary of the test data is in Appendix A, and those values were used in code calculations that were compared with laboratory experiments on the same rock.

Laboratory experiments were of two kinds: static indentation tests to verify the constitutive relations, and cutting tests to evaluate the dynamic predictions of the model. The static tests used a flat-bottomed punch to indent rectangular blocks of Berea sandstone confined by pressure plates on the sides (fig 3.2). The qualitative comparison of the crack configurations showed that the model captured the basic crack behavior (fig 3.3) and the quantitative comparison of the loads showed that the two failure criteria in the model bounded the actual loads (fig 3.4).

The model is less successful in predicting the details of drag bit cutting, and there are several reasons for this. First, the material is too complex to model perfectly and those deficiencies

may become more significant in a dynamic situation. Second, the stress criterion used for crack formation is affected by the pattern of the finite-element mesh; a fracture mechanics criterion would be better but much more complex. Third, the calculations are highly sensitive to the assumption of the contact area between the front surface of the cutter and the ledge of rock before it. During experiments this area changes constantly and it is almost speculative to assume an initial condition configuration. A possible solution is to model the cutter moving a significant distance through the rock, but this would require re-mesh capability and chip ejection in the code. Although conceptually possible, the size of the problem and the required computing time are formidable.

It appears that the basic physics of the rock cutting process is captured in this model. The correlation of load with depth of cut; the cyclic load variation during chip formation (see section 4 for experimental data); and the predicted tensile cracks dipping in the direction of cutter movement are all consistent with the actual results. Furthermore, all of the cutting tests were done under atmospheric conditions and thus had no confining pressure. Some of the inaccuracies of the model, such as the tensile crack propagation under a stress criterion, will be suppressed with the confining pressures that represent real drilling conditions. More detailed descriptions of this work appear in References 9 - 11.

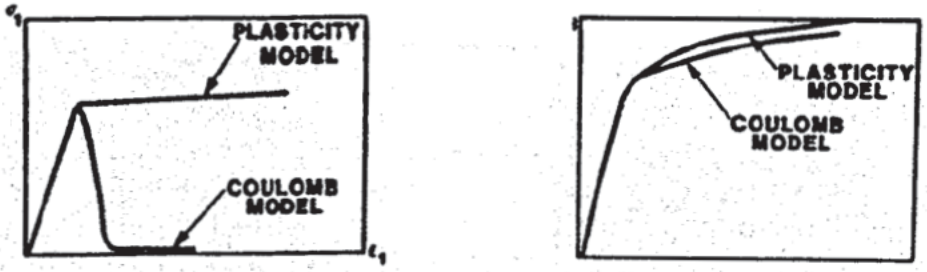

(a) Unconfined compression (b) Confined compression

Figure 3.1 -- Postfailure behavior of models

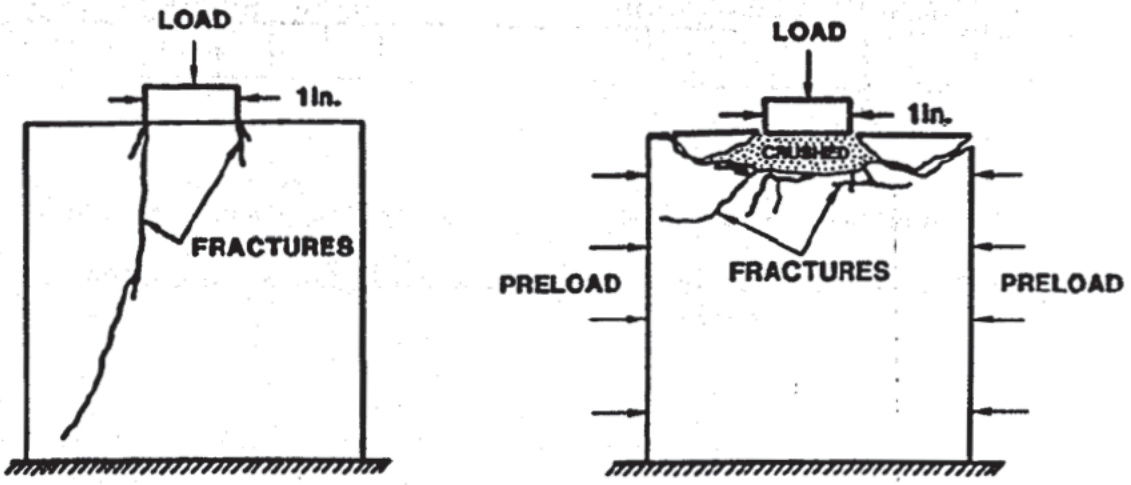

(a) Zero prestress (b) -2100 psi prestress

Figure 3.2 -- Fracture patterns in laboratory indentor tests

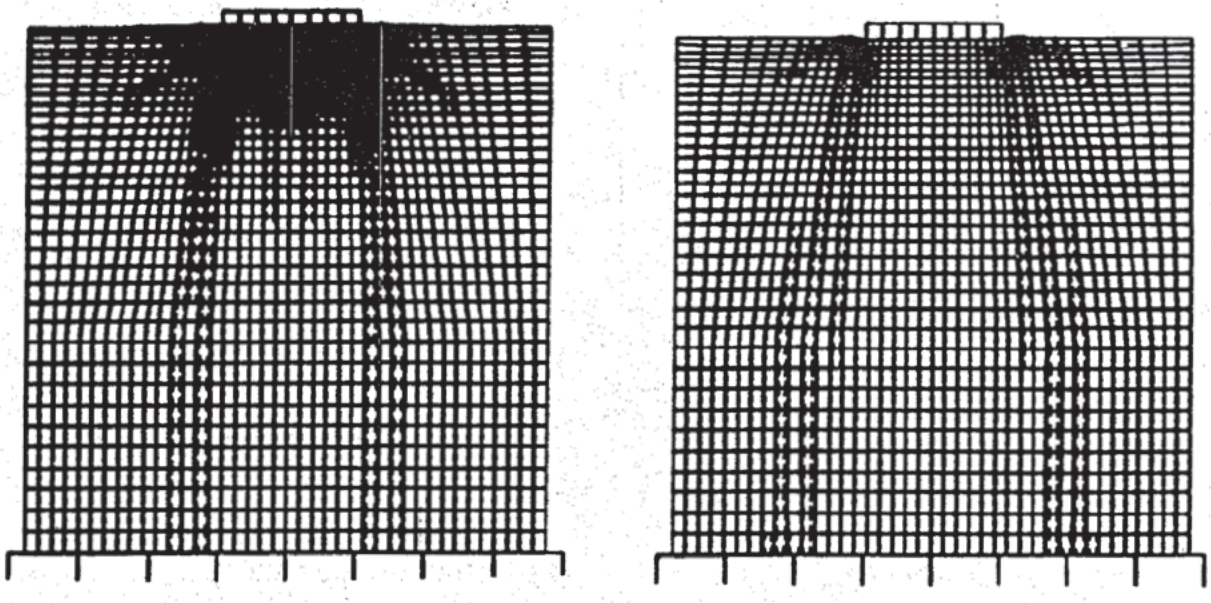

(1) Tensile/Coulomb model (2) Tensile/plasticity model

Figure 3.3a -- Predicted indentor fracture patterns (zero prestress)

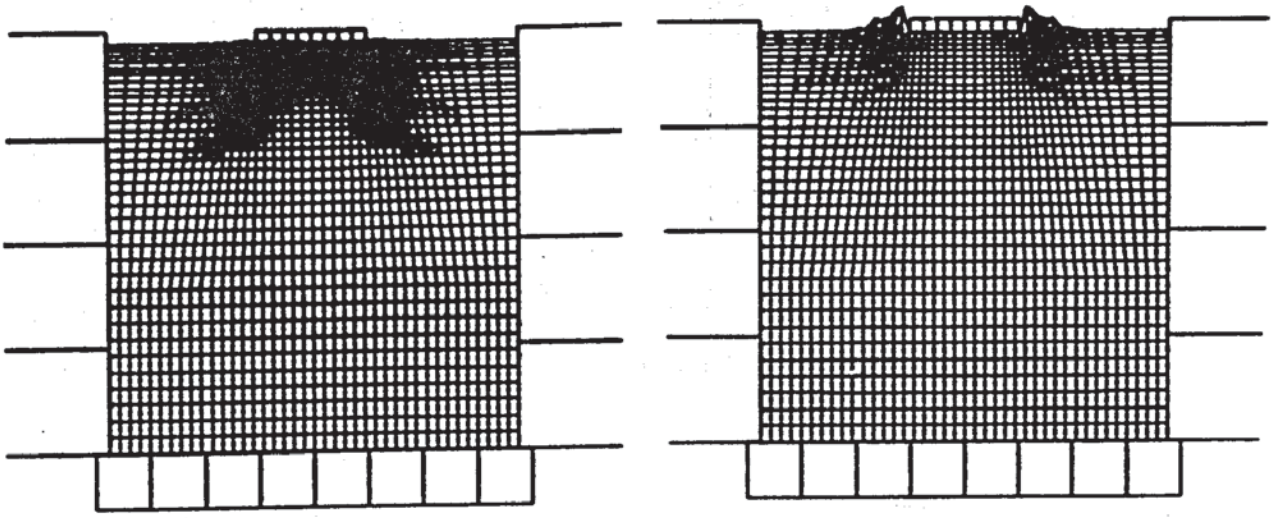

(1) Tensile/Coulomb model (2) Tensile/plasticity model

Figure 3.3b -- Predicted indentor fracture patterns (-2100 psi prestress)

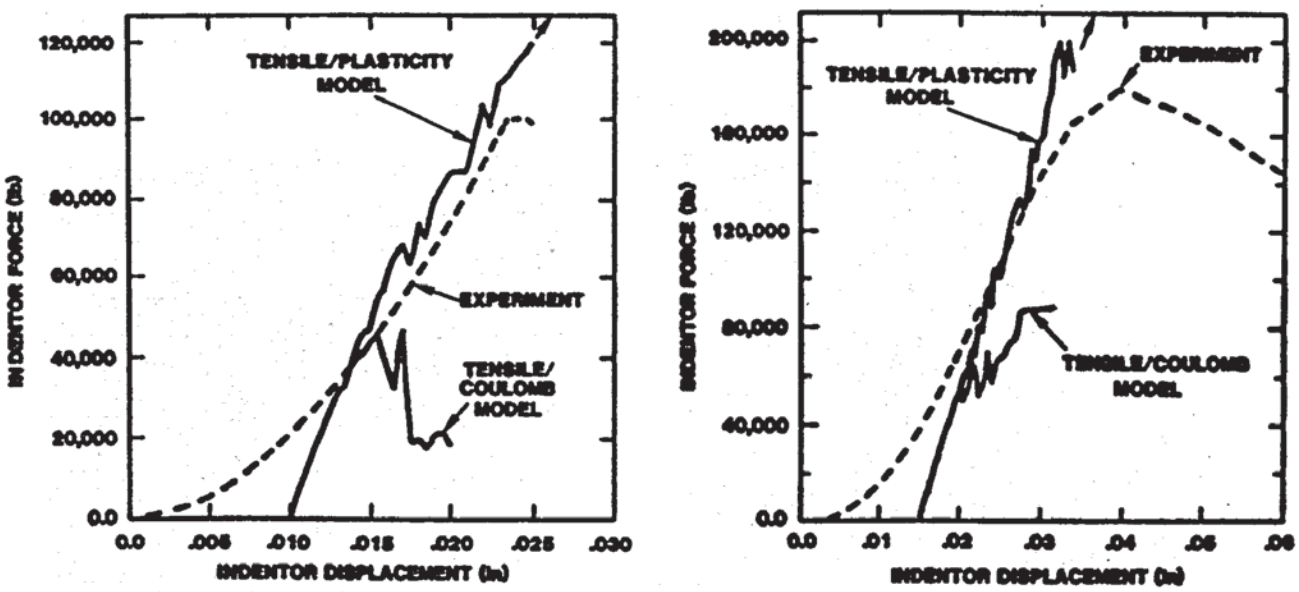

(a) Zero prestress (b) -2100 psi prestress

Figure 3.4 -- Comparison of predicted and measured indentor loads

4 -- SINGLE CUTTER TESTS

In a project that was parallel and complementary to the analytical modeling (section 3), we did many tests in which we passed a single PDC cutter through a rock sample and measured the forces on the cutter in three perpendicular axes. The apparatus for these tests was a modified milling machine that carried the rock sample on its moving table and fixed the dynamometer-mounted cutter in the position of the tool holder (fig 4.1). Depth of cut is very easily changed and the linear speed of the table can be varied up to a maximum of about 2 in/sec. The variables that we changed most often were type of rock, depth of cut, and cutter configuration (sharp or worn).

We also made several early attempts to see the chip formation as we collected force data. Both still and high-speed movie cameras were used to photograph cutting tests, but neither technique gave satisfying results. Cutting samples of birefringent plastic illuminated by polarized light gave typical photoelastic fringe patterns that confirmed the shape of the stress field in the plastic, but its properties were too different from rock to yield more than qualitative insight.

The most useful tests were of two kinds: measuring forces on the cutters and examining damage patterns in the cut rock. We must emphasize that we conducted all tests under atmospheric pressure, and neither the forces nor the damage patterns are like those same phenomena in rock under confining pressure. This does not negate our assumption that atmospheric tests, while not ideal on an absolute basis, are useful to compare different rocks and different cutting conditions.

Continuous force data showed a fairly periodic character in which the shapes of the vertical and horizontal force component plots were essentially identical (fig 4.2). When the cutting speed was correlated with the time axis to give distance that the sample moved between the force peaks, these distances roughly matched the intervals of the periodic dipping fractures observed in the damage analysis (see below). This phenomenon agrees with a chip formation

model in which forces increase as the chip-boundary crack propagates through the rock ahead of the cutter, and then decrease as the chip detaches and the cutter moves into the now-vacant space.

Force data provided experimental input to several other projects. The mechanical model (section 3), the thermal model (section 7), the complete bit design model (section 9), and the drillstring dynamics model (Ref 12) all used single-cutter data in their respective calculations. The force measurements also gave some insight into the physics of the cutting process. Many of the effects were quite intuitive: forces increased with depth of cut; stronger rocks gave higher forces; worn cutters required more force than sharp ones. A sample of typical measurements appears in Table 4.1. It is clear from the data in the table that deeper cuts are more efficient (less work per volume of rock removed) and that the ratio of vertical to horizontal force does not vary greatly between worn and sharp cutters. The latter result seems wrong if cutting forces are generated primarily by the front surface of the cutter, but if the cutter is seen as an indentor moving through the rock the data appear more reasonable.

One departure from the normal practice of using virgin rock in the experiments was a series of tests in which a cut was first made in an undamaged surface and a second cut was overlaid in the area damaged by the first cut (Table 4.2). In general, the forces were higher for the second cuts, but so were the volumes of rock removed. The average particle size of the chips was also smaller in the second cuts (Table 4.3). There appear to be at least four effects in play here, two of which tend to increase forces in the damaged areas and two which decrease them. Since more rock, of a smaller average particle size, is removed in the second cuts, more free surface is created. The existing cracks also inhibit the propagation of cracks nucleated by the cutter tip on the second pass. Both of these would increase the force required to remove the rock, but the existing cracks also provide some of the free surface for the new chips and relieve the compressive region at the cutter tip, thus easing the nucleation of new cracks. The two latter phenomena apparently dominate.

We examined the damaged rock in two ways (Ref 13): after the samples were cut, they were impregnated with dye and sectioned to look at the fracture patterns; and as each cut was made, the chips were collected and examined for size and shape. The crack configuration in the rock samples was in good agreement with the shapes predicted by the analytic model (fig 4.3) and the extent of the damage was related to the depth of cut, i.e., greater forces produced longer cracks. When we view the sectioned rock sample in the direction of the cut, we also see that the damage extends to each side of the cut (fig 4.4). The extent of the lateral damage may be important in considering the overlapping cuts made by a drill bit. Crack patterns left by the cutters were basically the same in three kinds of rock -- Westerly granite, Vermont marble, and Tennessee marble. Microscopic examination of various individual cracks did not show any shear displacement, indicating that they were indeed tensile.

The chips themselves were mostly thin, flat, and concave downward (fig 4.5), which is generally contrary to the way chip formation is sketched in the literature (fig 4.6). Chip shape was remarkably consistent in different rocks and with different cutters (fig 4.7). Length of the major chips was also approximately equal to the spacing of the subsurface cracks and the force peaks. Virtually all of the larger chips had a crushed, powdery zone on the trailing edge, which indicates a region of intense triaxial compression. This also implies a chip formation process in which the cutter acts as a moving indentor. Thus there is a compressive zone at the cutter tip, surrounded by a tensile zone that nucleates a crack ahead of the cutter. This crack runs toward the free surface, relieving the compression at the cutter tip and extending the chip boundary forward until the chip is detached by the bending moment from by the cutter tip.

The single cutter tests described in this section have been aimed at understanding basic chip formation processes and at providing baseline numerical values to be used in other calculations. The cuts have been short and slow. Many other tests,

described in later sections, have incorporated longer runs at higher speeds for realistic evaluation of cutter wear and heating.

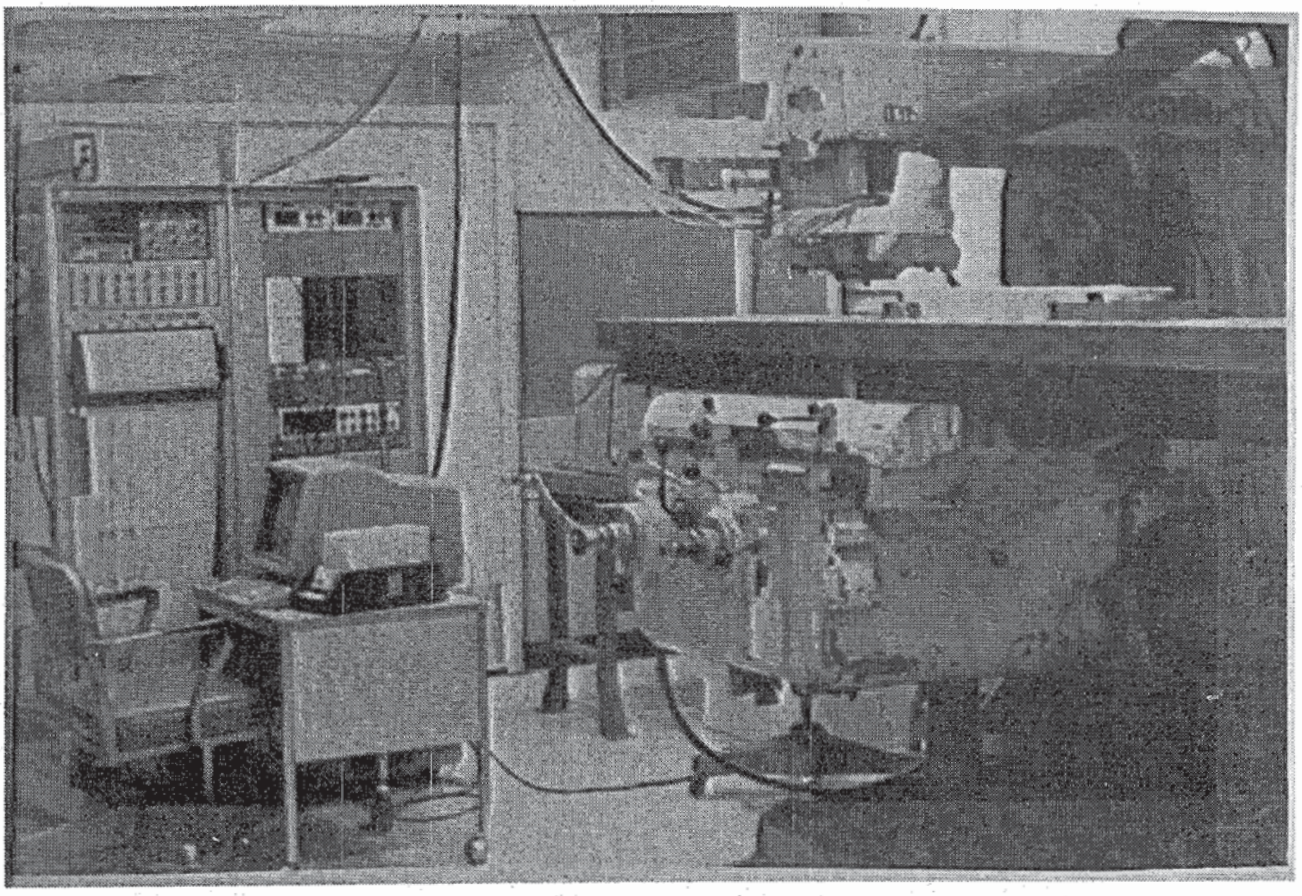

Figure 4.1 -- Modified milling machine used for single cutter tests

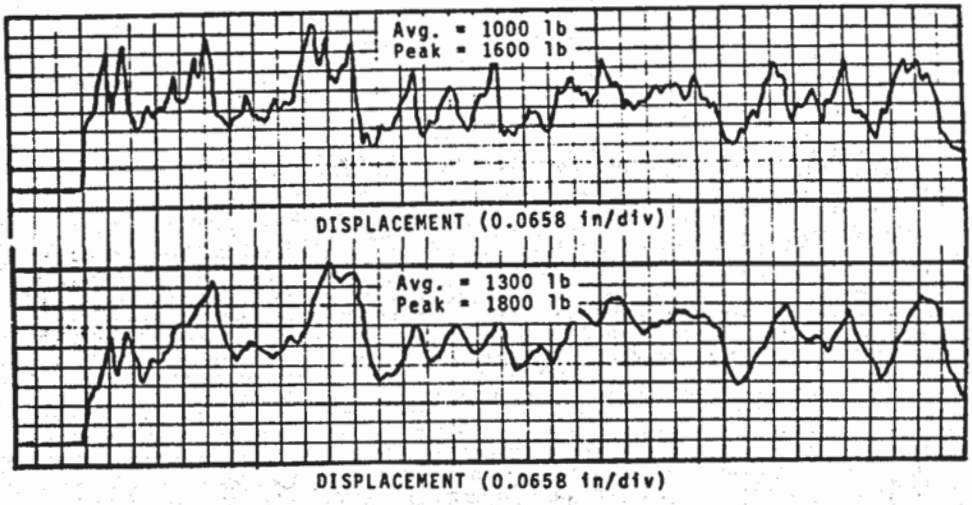

Figure 4.2 -- Horizontal (top) and vertical (bottom) forces for a typical cut. Force scale is 200 lb/division.

Table 4.1a -- Data from a series of cuts in Berea sandstone (unconfined compressive strength = approx. 8,000 psi)

Depth of Cut, in.	Cutter Shape Sharp Worn	Cutter Engagement F = Full H = Half in Previous Cut	MEAN FORCES, lb (STD DEVIATION) X, Direction	Y, Lateral of cut	Z, Vertical	X/Z	Area of cut, in^2	Index of Work per cut Volume, ft.-lb/in^3
.030	S	F	32.5 (14.0)	-.2 (2.27)	27.9 (10.2)	1.16	.0048	564
.050	S	F	46.7 (28.7)	0 (3.2)	38.2 (20.7)	1.22	.0103	378
.050	S	H	27.9 (17.7)	-3.4 (3.0)	23.4 (12.9)	1.20	.0072	323
.100	S	F	109.7 (74.3)	-.1 (6.2)	83.5 (56.2)	1.31	.0288	317
.100	S	H	39.9 (27.0)	-6.4 (5.1)	32.8 (19.6)	1.22	.0190	175
.030	W	F	59.9 (14.4)	-1.3 (2.0)	68.2 (12.2)	.88	.0100	499
.050	W	F	79.7 (30.6)	-1.2 (3.1)	84.2 (24.3)	.95	.0178	373
.050	W	H	40.1 (17.4)	-4.8 (3.0)	42.3 (12.9)	.95	.0098	341
.100	W	F	122 (72.9)	-4.2 (5.6)	120 (52.7)	1.02	.0397	236
.100	W	H	50.4 (30.8)	-8.9 (5.6)	49.0 (52.7)	1.03	.0226	186

BEREA SANDSTONE
UNCONFINED COMP.
STRENGTH ~ 8000 psi

Table 4.1b -- Data from a series of cuts in Westerly granite (unconfined compressive strength = apprx. 33,000 psi)

Depth of Cut, in.	Cutter Shape Sharp Worn	Cutter Engagement F = Full H = Half in Previous Cut	MEAN FORCES, lb (STD DEVIATION) X, Direction	Y, Lateral of cut	Z, Vertical	X/Z	Area of cut, in²	Index of Work per cut Volume, ft.-lb/in³
.025	S	F	113 (35.5)	-4.3 (6.6)	137 (33.2)	.82	.0036	2616
.050	S	F	217 (101)	-8.0 (13.1)	230 (76.0)	.94	.0103	1756
.050	S	F	239 (75.4)	-4.5 (16.2)	315 (76.7)	.76	.0103	1934
.050	S	F	341 (113)	-7.6 (21.1)	417 (100)	.82	.0103	2759
.050	S	H	128 (44.7)	-48.2 (15.0)	169 (49.1)	.76	.0072	1481
.100	S	F	576 (251)	-14.5 (30.1)	611 (187)	1.08	.0288	1667
.100	S	H	313 (118)	-83.6 (31.6)	432 (128)	.72	.0190	1373
.025	W	F	631 (17.4)	-16.5 (128)	1017 (188)	.62	.0081	6492
.050	W	F	898 (139)	-20.6 (15.3)	1342 (199)	.67	.0178	4204
.050	W	H	454 (115)	-44.6 (18.3)	658 (151)	.69	.0098	3960
.100	W	F	920 (209)	-261 (66.1)	1242 (393)	.74	.0397	1931
.100	W	H	563 (209)	-153 (43.3)	775 (260)	.73	.0226	2076

WESTERLY GRANITE
Unc. σ ~ 33,000 Psi

Pairs of runs	Average force, lb.	Weight of cuttings, gm.	Specific rock removal, mg/J	Ratio of second run to first
1a	456	3.228	10.45	
1b	530	3.432	9.56	0.92
2a	480	3.665	11.28	
2b	459	4.155	13.36	1.20
3a	510	3.819	11.04	
3b	528	4.648	12.98	1.17
4a	473	3.239	10.09	
4b	543	4.544	12.35	1.23

Table 4.2 -- Comparison of paired runs through virgin and pre-damaged rock (Tennessee marble)

Mesh size, um	First run	Second run
4000	77.6	80.7
2000	54.7	57.7
1000	35.8	37.9
500	24.6	25.7
250	15.0	15.5
125	8.4	9.0
30	2.2	2.6

Table 4.3 -- Percentage of total cuttings passing through a given mesh size (average of four runs)

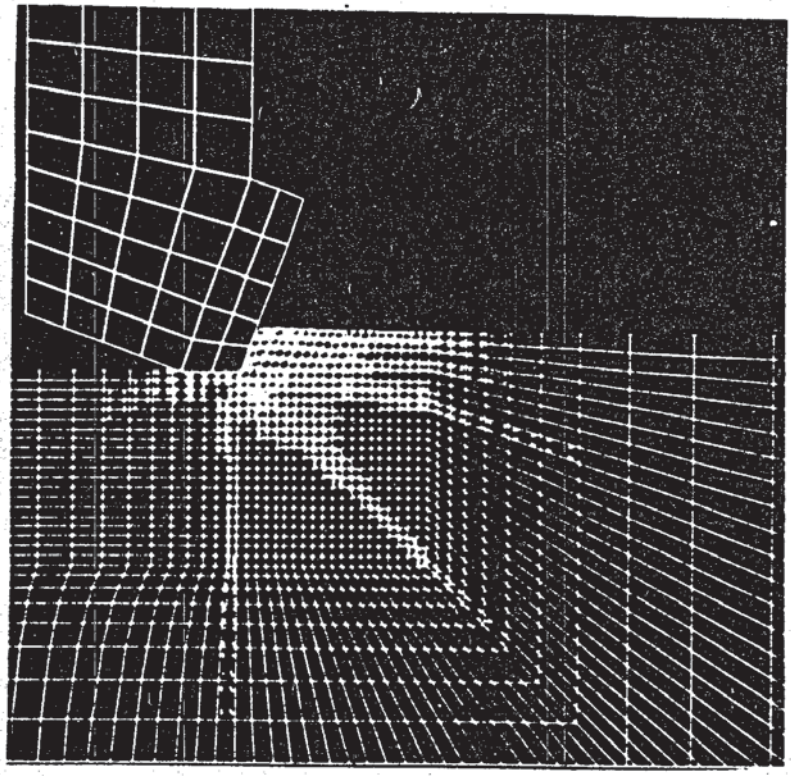

Figure 4.3a -- Finite-element-code prediction of fracture development during cutting

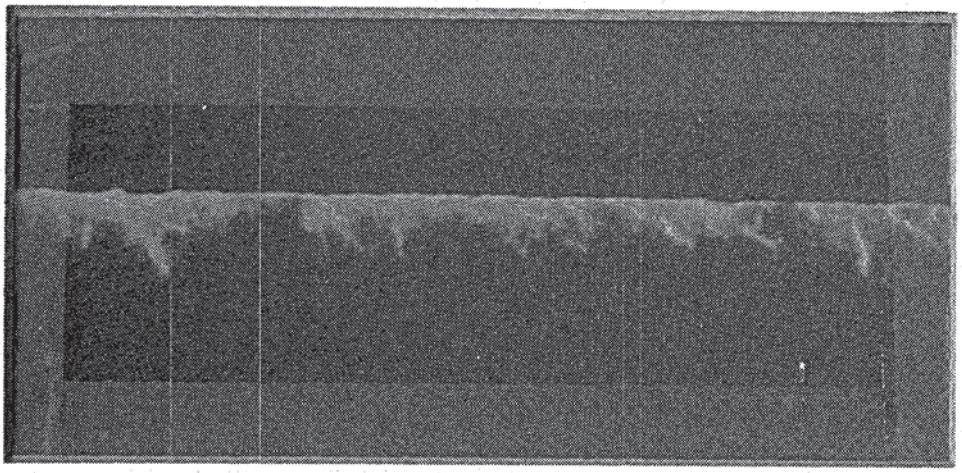

Figure 4.3b -- Photograph of rock specimen impregnated with fluorescent dye and sectioned along the cut track (direction of cut is left to right)

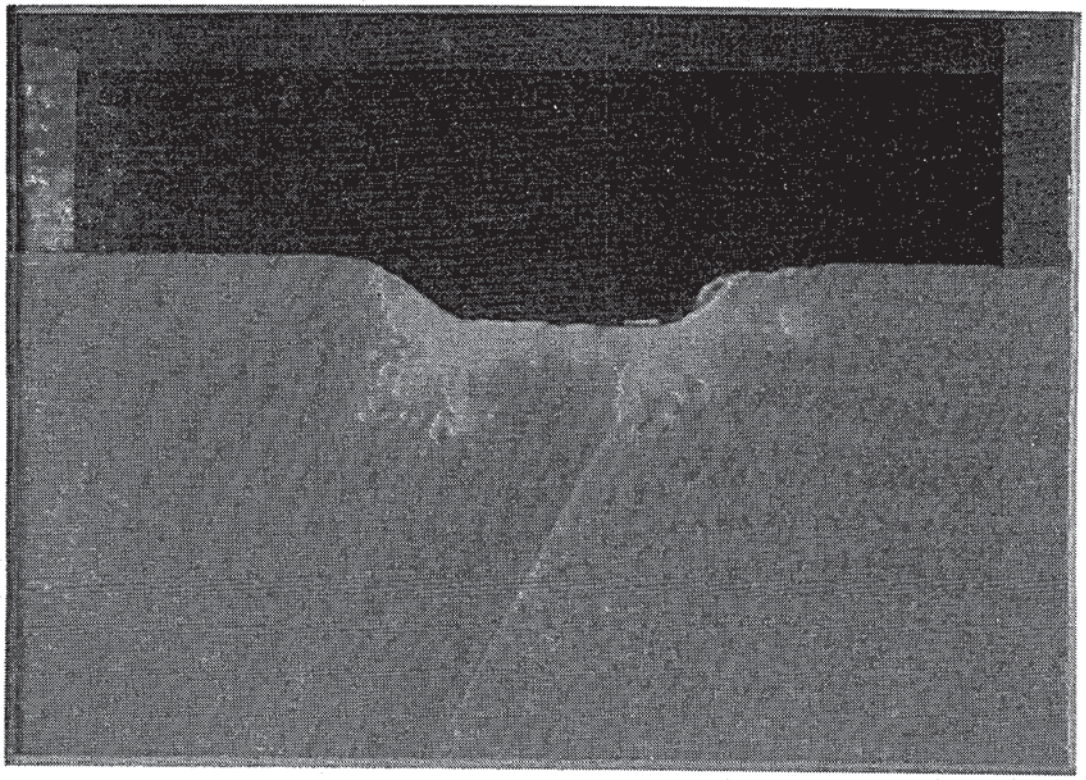

Figure 4.4 -- Damage pattern extending laterally from the cutter track. Direction of cut is normal to the page.

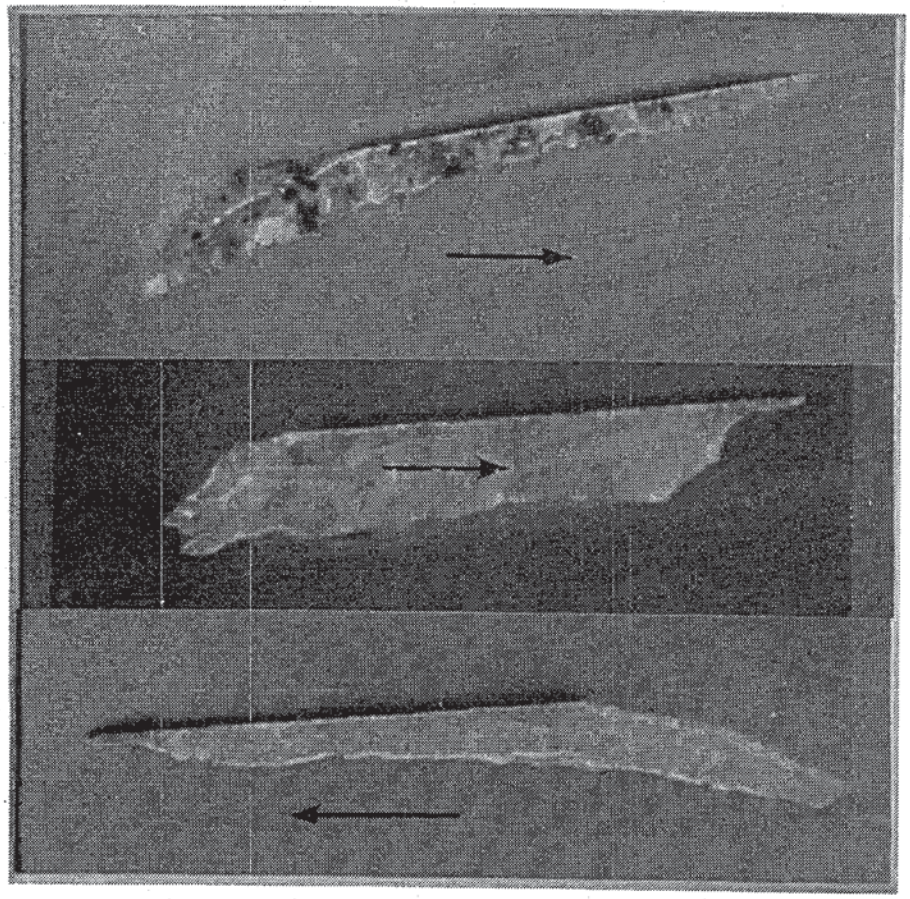

Figure 4.5 -- Profiles of typical chips (arrows show cut direction)

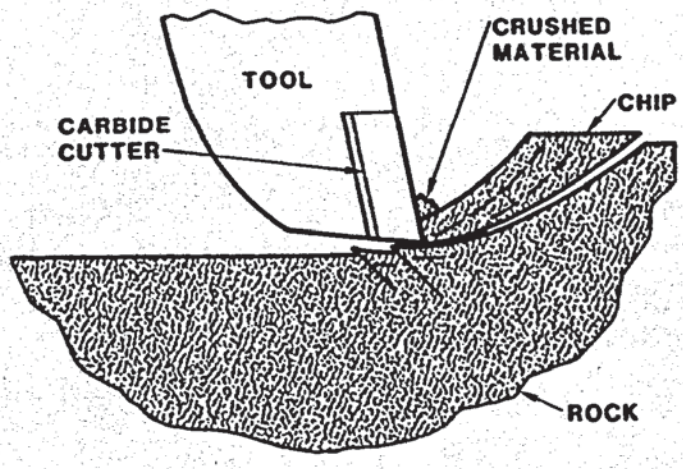

Figure 4.6 -- Chip formation as typically represented in literature

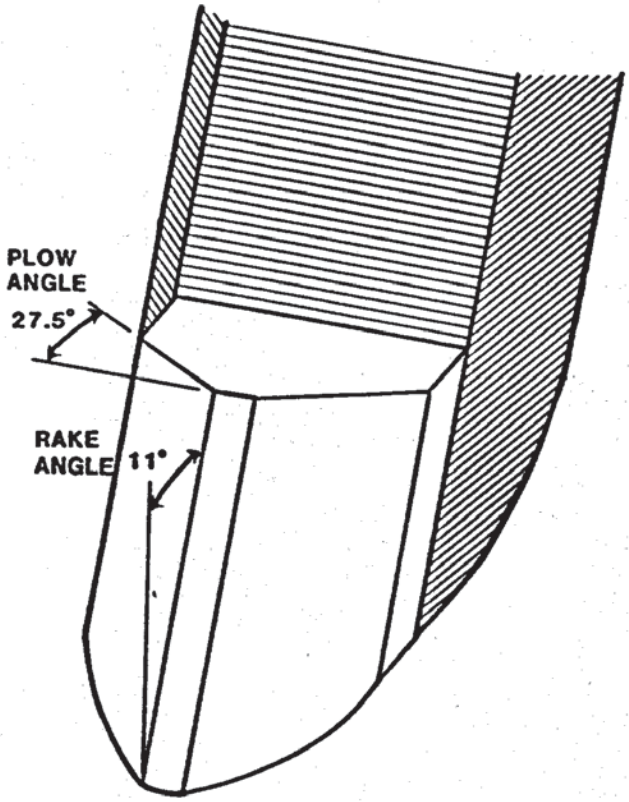

Figure 4.7a -- Sketch of coal mining cutter

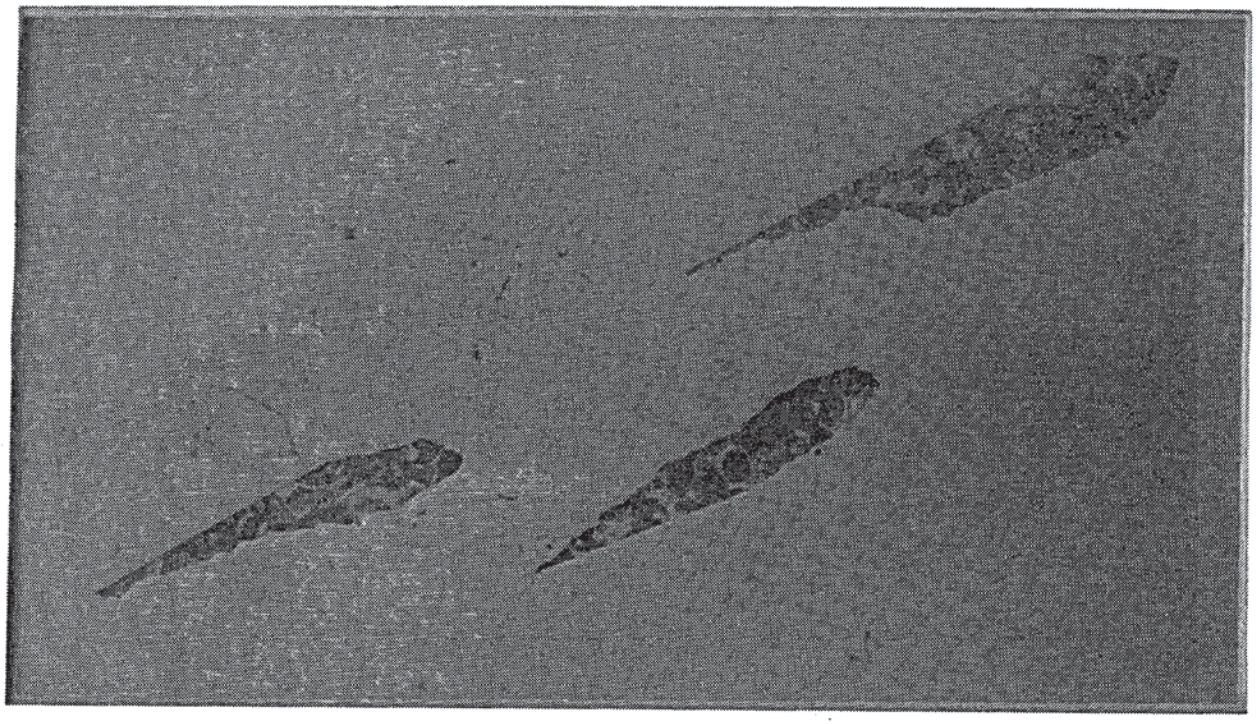

Figure 4.7b -- Chips from single cutter test with coal cutter

5 -- BIT HYDRAULICS

Our investigation of PDC bit hydraulics had two major goals: an understanding of the fluid flow paths across the bit face, and numerical values for the convective heat transfer coefficients from the cutters to the fluid. The nature of the flow path is important because it identifies, in a qualitative way, stagnant areas of fluid that cause poor cleaning and cooling. Heat transfer coefficients give an upper bound to the amount of heat that the drilling fluid can carry away from the cutter and thus help to determine its temperature. A complete description of this work is in Reference 14.

Because the flow field around a typical PDC bit is so complex, it is virtually impossible to write an analytic description of it. The alternative is flow visualization using a model bit and fluid to simulate actual drilling. Conventional drilling fluids are essentially opaque, but we can use clear water in the experiments if we use similitude equations to modify the flow conditions.

The major piece of equipment used in this work is the bit hydraulics test stand shown in figure 5.1. Its principal components are a rotating vertical drive shaft, a bit on the lower end of the shaft, a transparent simulated wellbore around the bit, and a flow loop that sends the fluid down the inside of the drive shaft, through the bit nozzles, back up the annulus, and through a manifold that returns it to the pump. Bits up to 17 inches in diameter can be turned as fast as 900 rpm and the complete flow path can be pressurized to 750 psi.

First attempts to look at the flow paths used dye streams injected through the bit nozzles. Dispersion and diffusion of the dye made the flow path boundaries unclear, however, so we abandoned this technique. A more successful, although more laborious, method was high-speed photography of 3 mm polystyrene pellets in the stream. Frame-by-frame analysis of the film then revealed the trajectory of each bead. Since the film moved at constant speed, the distance between pellet positions on succeeding frames was

proportional to the pellet velocity, and areas of stagnation and recirculation were obvious.

The 6.5-inch bit used in these tests had 10 nozzles and we examined three flow configurations for comparison: (1) all nozzles open, (2) only the four center nozzles open, (3) only the outer three nozzles open. Figure 5.2 shows sample flowlines for the three cases (the points plotted as open circles, not solid dots, are points of stagnation).

All the cutters on the test bit were also fitted with heat transfer gages, and the convective heat transfer coefficients were measured for the three nozzle configurations. Bit rotary speed varied from 0 to 120 rpm. Figure 5.3 shows how coefficients for a typical cutter varied with the rotary speed; figure 5.4 gives the differences in coefficients among the cutters at different locations on the bit; and figure 5.5 indicates the variation in heat transfer coefficient with Reynolds number.

Some general conclusions about the effects of nozzle configuration and rotary speed can be reached:

Measurement of the convective heat transfer coefficients is very useful. It not only enables us to calculate cutter temperatures, but it confirms the stagnation points seen in the flow visualization.

The flow pattern produced by the four center nozzles alone gave the highest velocities and the best cooling across the bit face.

Most severe stagnation was around the outer cutters. This is not unreasonable, since they are farthest from the nozzles, but it is important because this area is most vulnerable to poor cleaning and cooling.

The effects of rotating the bit were not significant. It is not clear whether that is unique to this bit design.

Information on PDC bit hydraulics was essentially nonexistent before these experiments. This is in contrast to roller-bit hydraulics, which has been extensively studied and reported. The heat transfer data collected here are indispensable in calculating

cutter temperatures and that, in turn, is the crux of optimizing bit life.

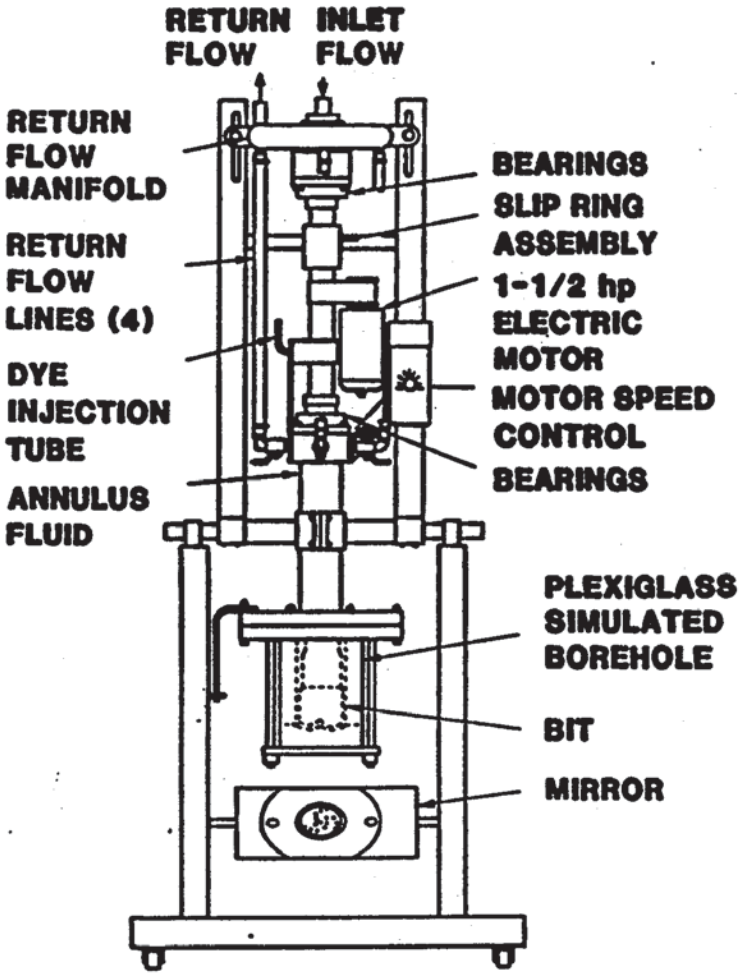

Figure 5.1 -- Bit hydraulics test stand

(a) (b) (c)

Figure 5.2 -- Typical pathlines for 3 bit hydraulic configurations: (a) all nozzles open, (b) only inner 4 nozzles open, (c) only outer 3 nozzles open

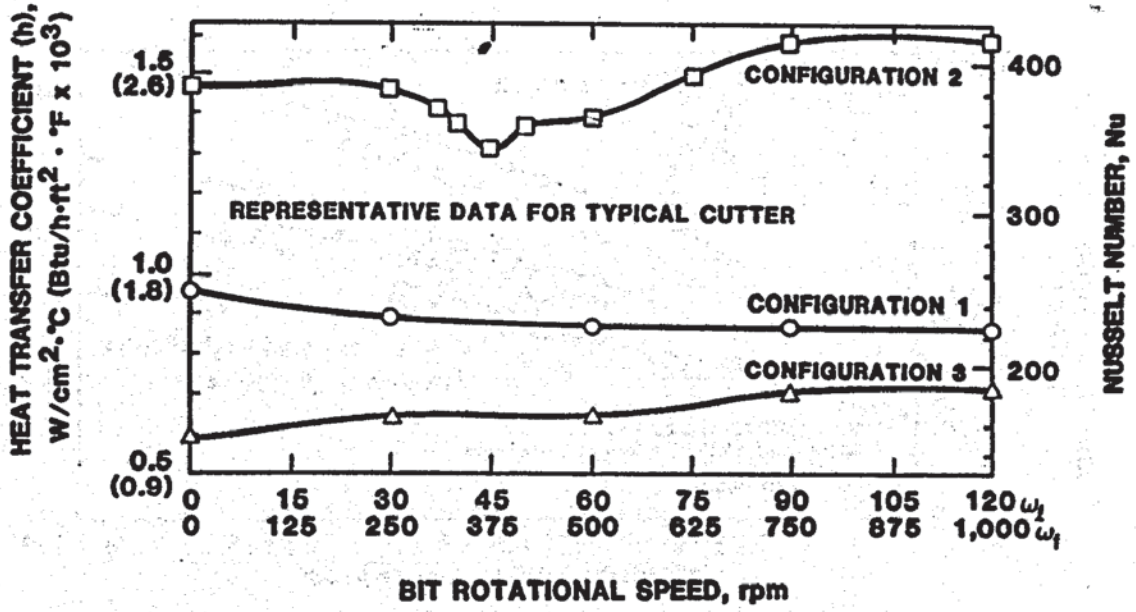

Figure 5.3 -- Variation of heat transfer coefficient with bit rotary speed and flow configuration

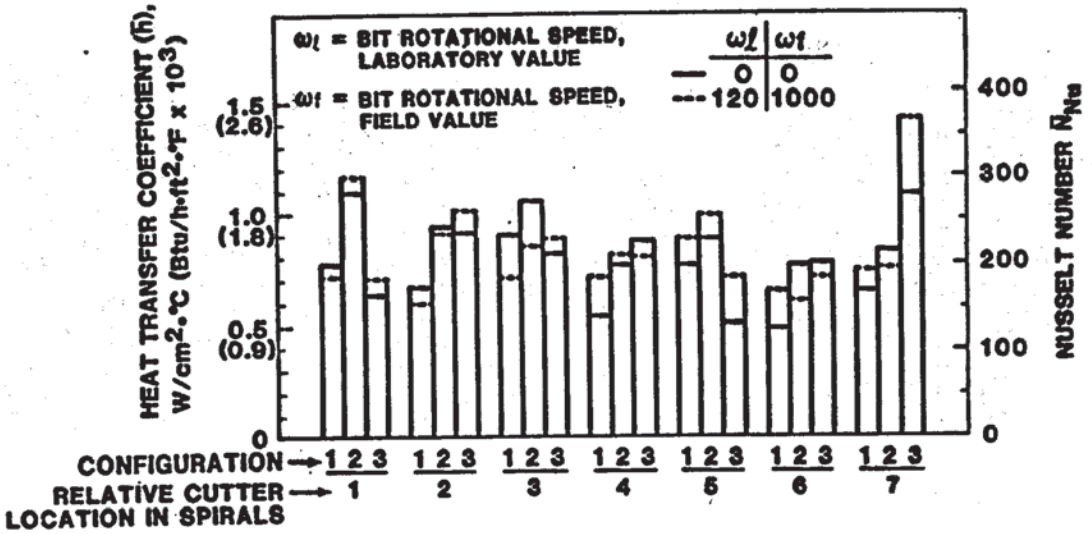

Figure 5.4 -- Variation of heat transfer coefficient with cutter position on bit

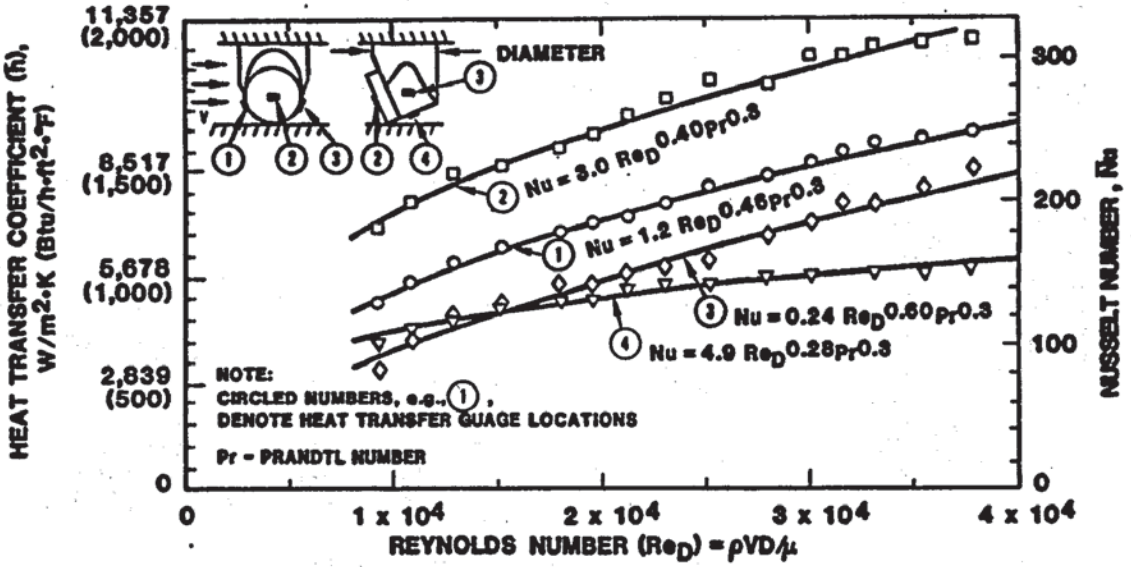

Figure 5.5 -- Variation of heat transfer coefficient with Reynolds number and position on stud

6 -- WEAR AND FRICTION TESTS

General Electric Corporate Research and Development, under contract to Sandia, carried out a series of tests in which they used single PDC cutters to make long continuous kerfs in various rocks at various cutting speeds. Reference 15 is a complete description of this work. These tests provided data on wear mechanisms, wear rates, and coefficients of friction between the rocks and the cutters (described in this section), and on temperature distributions in the cutters (described in section 7). Because the tests lasted long enough to measure wear and wear rates, the data represents a range of cutter conditions (sharp to badly worn). The cooling conditions for the cutters also varied from dry cutting through several flow rates.

The basic tool used in these experiments was a 54-inch vertical turret lathe (fig 6.1) that could spin a block of rock approximately three feet square by 1 1/2 feet thick, and that had cutters mounted in a tool holder that traversed the rock's top surface. Since the rotary speed of the rock stayed constant for a given experiment, the cutting speed decreased from 7.8 feet/sec to 1.3 feet/sec as the cutter moved inward from the largest to the smallest radius.

The most important measurement was that of wear rate, that is, the volume of cutter material removed per distance cut. The top surface of the rock was divided into six concentric bands of equal width (2 inches) separated by plunge cuts deeper than the test cuts. A different cutter was used for each circular band and data for each cutter were assigned to the average speed for its band. Depth of cut, 0.020 inch, was uniform for all bands, and all of the wear tests were done in Nugget sandstone.

Decrease in cutter volume was calculated from the increase in wearflat dimensions; this was measured under a low-power microscope after each run. When the wear volume data (for all speeds) are plotted as in figure 6.2, the points for the dry cuts fall very nicely on a straight line and the points for the wet cuts (with coolant flood around the cutter) fall on two separate but similar

straight lines. The slope of the curve (i.e., wear rate) for the dry cuts is at least an order of magnitude greater than those of the wet cuts. This seems to imply several effects:

The wear mechanisms for the wet and dry cuts are different, but neither case is significantly affected by cutting speed. This is consistent with the principle that wear is proportional to rubbing distance as long as the wear mechanism remains the same. Optical microscopy of the wear scars on the cutters also showed that the wet cut wear was by abrasive microchipping of the individual diamond grains, while the dry cuts produced severe thermal damage, including grain boundary weakening and whole-grain pullout.

The lower straight line in the wet-cut data represents the wear rate for two intermediate cutting speeds (6.2 and 5.1 feet/sec), but this is not intrinsically reasonable. It is hard to imagine a mechanism which would produce higher wear rates at both higher and lower speeds. A more likely explanation is that lack of uniformity among the materials of individual cutters led to higher wear rates in some of them.

Thermal modeling described in the next section shows that higher heat flux into the wearflat radically changes the temperature distribution in the cutter and leads to increased thermal stresses that accelerate wear. Differences in heating between wet and dry cuts have two probable causes -- the liquid coolant reduces the coefficient of friction between the cutter and the rock, thus lowering the heat input, and the liquid has a much higher convective heat transfer coefficient, thus increasing the heat carried away from the cutter.

The most important result of the wear tests, which is emphasized in section 9, is that wear mechanisms change drastically with different cutting conditions. The parameter that signals this change is average wearflat temperature; when it exceeds 350°C, the wear rate increases by at least an order of magnitude.

Because the heat input to the cutter comes from the rubbing friction on the rock, the coefficient of friction between the cutter and the rock is clearly a controlling variable in determining the temperature profile in the cutter body. To gain more data on how the coefficient changes, GE also did a series of tests measuring the friction forces at different cutting speeds, with different drilling fluids, in different rocks. A complete test matrix appears in Table 6.1.

The same vertical turret lathe used for the wear tests was again employed for the friction experiments, but the cutting conditions were somewhat different. Since we wanted to measure friction forces at constant speeds, the spiral cuts used in the wear tests were not appropriate. Instead, a circular rib of rock as wide as the cutter wearflat (fig 6.3) was isolated by a plunge cut on each side and the cutter was pressed against this without traversing. After following this procedure on the first test, we found that the rock wear rate was so low that subsequent cuts could be made on the unaltered flat surface.

The cutters were "worn", meaning that they had wearflat areas of approximately 0.03 square inches, and the diamond cutting edges were deliberately dulled to minimize the amount of rock removed. Part of the test matrix called for a higher cutting speed (16.5 feet/sec) than was previously possible, so the lathe was rewired to allow this. Vertical forces on the cutters were about the same as those in the earlier wear tests.

A complete summary of the friction test results appears in Table 6.2 and requires some comment. The diversity of cutting combinations makes generalizations difficult, but some conclusions do appear:

Sandstone had notably low friction using liquid drilling fluids, with the exception of diesel oil at high cutting speed. It was also the only rock with significant porosity, so it appears that the pores acted as fluid reservoirs and increased the chances that the cutter was riding on a liquid film. In the case of the high speed cuts, the higher wearflat temperatures could have vaporized the diesel more readily than the water or mud.

The diesel oil was not, in general, a better lubricant than water or mud. That, again, could be a result of its tendency to vaporize, aggravated by its lower specific heat relative to water.

Coefficients of friction mostly stayed the same or decreased as cutting speed increased. It is reasonable to believe that the higher interfacial temperatures in the high-speed tests were enough to alter the mechanical and perhaps chemical nature of the sliding contact. This is supported by the fact that four of the five tests that damaged cutters enough to require replacement were at high speed.

Higher friction coefficients with air were not surprising. Lack of lubrication contributed directly to higher forces, and may have had an indirect effect because of the higher temperatures.

The cutter wearflats showed several different effects after the tests. Most of these related to the debris that was packed on the flats and to the way that rock powder appeared to be thermally altered. Both effects varied with the drilling fluid, and it seems likely that they would vary even more if the drilling fluid were under borehole pressure. The nature of the fines collected on the wearflats seems to affect at least the friction coefficient and the mean stress on the rock.

Although there are many variables in the determination of friction coefficients, the values obtained in this series of tests are useful and representative of a wide range of actual drilling conditions. Better knowledge of friction coefficients will be crucial in improving our ability to predict changes in drill bit performance.

These tests, measuring wear rates and friction coefficients, have been important in providing numerical values for analytical modeling, in illuminating some fundamental performance changes at different drilling conditions, and in spotlighting some areas where further work would be fruitful.

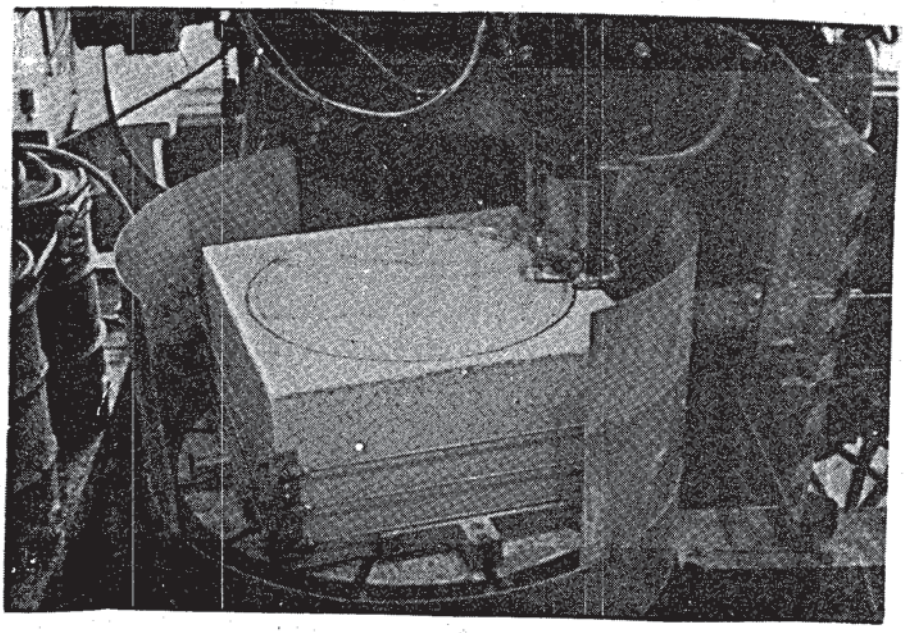

Figure 6.1 -- Vertical turret lathe used in GE's cutting experiments

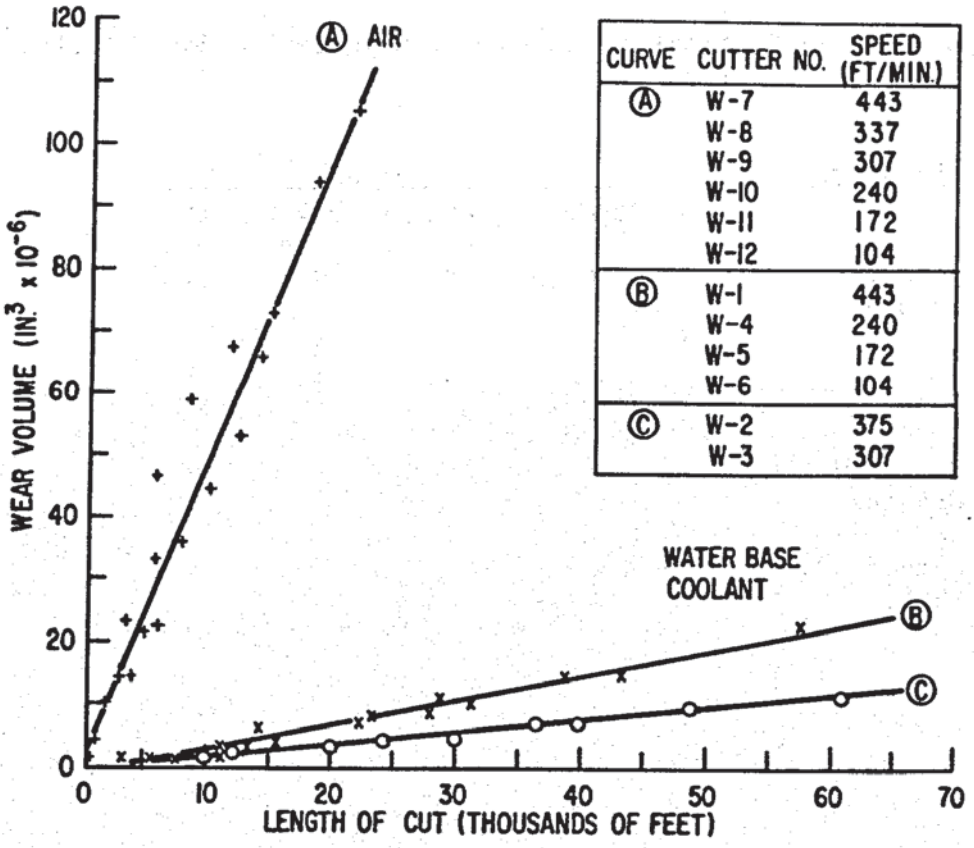

CURVE	CUTTER NO.	SPEED (FT/MIN.)
Ⓐ	W-7	443
	W-8	337
	W-9	307
	W-10	240
	W-11	172
	W-12	104
Ⓑ	W-1	443
	W-4	240
	W-5	172
	W-6	104
Ⓒ	W-2	375
	W-3	307

Figure 6.2 -- Cutter wear (volume) as a function of distance cut

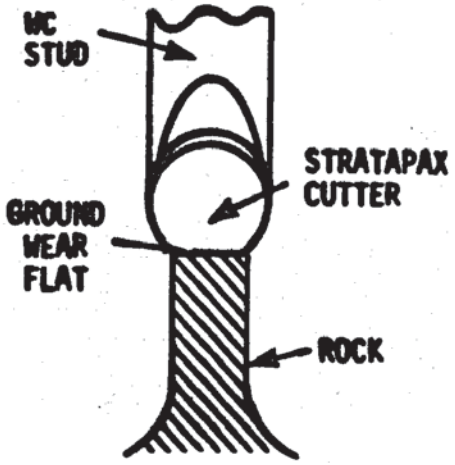

Figure 6.3 -- Original rock/cutter configuration for friction tests

Rock type	Coolant			
	Water	Mud	Oil	Air
Tennessee Marble	x	x	x	x
Nugget Sandstone	x	x	x	x
Sierra White Granite	x			x
Mancos Shale	x			x

Table 6.1 -- Test matrix for friction measurements

Table 6.2 -- Summary of data from friction measurements

Test Number	Cutter Number	Rock* Type	Fluid**	Rubbing Speed (m/s)	Friction Coefficient	Number of Data Points	Maximum Thrust Force (lb.)	Average Stress Normal to Rock Surface (psi)	Rock Wear Rate (in/rev)	Comments
18	SX-2	marble	water	1.00	0.20	73	579	7795	0.0010	
19	SX-2	marble	water	5.00	0.15	30	670	8824	0.0010	
20	SX-2	marble	air	1.00	0.33	99	613	5488	0.0007	
21	SX-2	marble	air	5.00	0.17	43	624	5594	0.0006	Excessive drill blank substrate wear. Diamond layer chipped at diamond-substrate interface. No thermal degradation of sintered diamond layer.
22	SX-70	marble	mud	1.00	0.20	58	797	8575	0.0008	
23	SX-70	marble	mud	5.00	0.10	37	849	10898	0.0005	
24	SX-70	marble	mud	1.00	0.13	76	729	8153	0.0006	
25	SX-70	marble	mud	5.00	0.11	26	967	10951	0.0006	
26	SX-70	s.s.	mud	1.00	0.04	66	845	11323	0.0007	
27	SX-70	s.s.	mud	5.00	0.04	47	768	7762	0.0009	
28	SX-70	s.s.	mud	5.00	0.04	43	631	8960	0.0006	
29	SX-70	s.s.	mud	1.00	0.03	23	647	12864	0.0005	
30	SX-70	s.s.	water	1.00	0.04	106	644	10363	0.0008	
31	SX-70	s.s.	water	5.00	0.06	49	612	8627	0.0008	
32	SX-70	s.s.	water	1.00	0.02	52	640	11234	0.0006	
33	SX-70	s.s.	water	5.00	0.04	29	562	9286	0.0007	
34	SX-70	s.s.	air	1.00	0.10	59	619	13774	0.0003	
35	SX-70	s.s.	air	5.00	0.30	31	446	4350	0.0001	Cutter red hot. Some chatter and vibration. Diamond layer thermally degraded at rubbing surface. No bulk degradation.
36	SX-15	granite	water	1.00	0.09	41	816	15313	0.0003	
37	SX-15	granite	water	5.00	0.05	28	902	16527	0.0003	
38	SX-15	granite	air	1.00	0.18	48	850	16335	0.0002	Cutter detached - poor braze joint. No thermal degradation.
39	SX-18	granite	air	5.00	0.18	21	703	10354	0.00009	Cutter detached - braze alloy melted. Diamond layer thermally degraded at rubbing surface.
40	SX-19	s.s.	diesel	1.00	0.05	69	791	14516	0.0006	
41	SX-19	s.s.	diesel	5.00	0.30	16	502	6608	0.0004	
42	SX-19	marble	diesel	1.00	0.34	36	480	10063	0.0005	
43	SX-19	marble	diesel	5.00	0.13	23	917	21544	0.0003	Only moderate thermal degradation of diamond layer.
44	SX-20	shale	air	1.00	0.17	27	457	7510	0.0003	
45	SX-20	shale	air	5.00	0.15	22	231	5073	0.00008	
46	SX-20	shale	water	1.00	0.09	18	506	7191	0.0005	
47	SX-20	shale	water	5.00	0.06	20	242	6158	0.0005	
48	SX-20	shale	air	1.00	0.11	28	364	6385	0.0011	
49	SX-20	shale	air	1.00	0.13	68	533	7322	0.0003	

*Rock Type
marble - Tennessee Marble
s.s. - Nugget Sandstone
granite - Sierra White Granite
shale - Mancos Shale

**Fluid
water - tap water
air - still air
diesel - No. 2 Diesel fuel flash point 150-160° F
mud - 20 ppb. Wyoming Bentonite
2 ppb. sodium polyacrylate
plastic viscosity=35.5 cp.
Bingham yield=17.5 lb/100ft^2
pH=8
weight=8.55 lb/gal

7 -- THERMAL MODELING AND EFFECTS

The importance of thermal effects on PDC cutter wear led us to do extensive work on the temperature and stress distributions in a cutter/stud assembly. This effort coupled analytical models with actual measurement of the temperatures within an experimental stud-mounted cutter. Maximum temperatures at the wearflat, sudden changes in temperature around the cutter, and steep temperature gradients in the assembly near the cutting edge all have significant effects on the wear rate.

There are several ways in which temperature affects wear rate. Reference 16 gives a detailed description of thermal and mechanical phenomena that promote wear, but we will give a brief summary here of the ones that primarily involve temperature.

First, the important parameter in the abrasive wear rate of metals is the ratio of the abrasive hardness to the metal hardness. If this ratio is less than 1.2, the wear mechanism is called "soft" abrasion and the rate is relatively insensitive to the ratio; if, however, the ratio exceeds 1.2, the wear is considered to be "hard" abrasion and the rate increases dramatically with the ratio. Assuming that quartz is the abrasive and tungsten carbide (WC) is the metal, the combination undergoes soft abrasion at room temperature, but as the wearflat gets hotter the tungsten carbide softens faster than the quartz and the wear rate accelerates in the hard abrasion mode. Because the hard but brittle diamond cutting surface requires the support of the WC substrate to absorb shock and prevent gross failure, the increased wear of the WC leads to increased wear of the entire cutter assembly.

Second, the decrease in fracture toughness of the tungsten carbide at increased temperatures means that the fatigue of cyclic loading and the stress waves from impact loading have a greater tendency to initiate and propagate fractures in that material.

Third, a cutter which has developed high temperatures at the rubbing interface will see large thermal stresses if the bit is suddenly lifted off bottom so that relatively cool drilling fluid is in contact with the hot wearflat. This situation can occur while

adding a new joint of drill pipe or when the drill string vibrations cause the bit to bounce off bottom. Severe drill string vibrations also increase the shock loading that can propagate cracks.

Analysis -- Temperature profiles within the cutter are determined by many variables: cutting force, cutting speed, wearflat area, friction coefficient between the rock and the cutter, thermal properties of the rock and of the cutter, convective cooling from the drilling fluid, and cutter geometry. It is clearly valuable to know the relative importance of these variables, and the way to do that is to write a mathematical description, or model, of the cutter.

In brief, the determination of the temperatures in the cutter assembly proceeds in the following steps: (1) calculate the heat generated by the friction between the cutter and the rock; (2) calculate the fractions of the heat going into the cutter and into the rock; (3) calculate the amount of heat removed from the cutter by convective cooling and by conduction into the bit body; (4) determine the equilibrium temperatures within the cutter assembly.

The idealized two-dimensional geometry shown in figure 7.1 is a finite element mesh based on a "standard" cutter, as shown in figure 7.2. The solution of the finite element problem was combined with a standard energy partition solution for a two-dimensional slider on a semi-infinite surface to yield the temperatures throughout the cutter assembly. Although the temperature gradients in the stud are important to evaluate thermal stresses (sample temperature profiles are shown in figures 7.3a and 7.3b), the most immediately useful quantity is the average wearflat temperature. The fundamental equation for this is

$$T_w = T_f + \frac{\mu F V f}{A_w [1 + \frac{3\sqrt{\pi}}{4} kf (\frac{V}{xL})^{1/2}]}$$

where the variables are defined:

f = thermal response function = $\frac{T_w - T_f}{q}$

q = frictional heat flux into the cutter wearflat

A_w = wearflat area

F = vertical force on cutter

k = thermal conductivity of rock

L = wearflat length (in direction of cut)

T_w = average wearflat temperature

T_f = drilling fluid temperature

μ = coefficient of friction between rock and cutter

V = cutter speed

x = thermal diffusivity of rock

The derivation of this equation is explained in detail in References 17 - 19, but its basic form is enough to show the relative importance of the variables. The thermal response function may require some comment: it represents an index of the temperature rise in the cutter for a given heat input, and its value is related to the thermal properties of the cutter materials, the cutter geometry, the temperature and heat transfer coefficient of the fluid, and the boundary conditions for cooling the cutter stud. The finite element solution gives this value and a sample of the results for different cutter configurations is shown in Table 7.1.

One important result of the ability to calculate the wearflat temperature is that the specification of a critical temperature, which must not be exceeded, leads directly to a critical weight-on-cutter for any given drilling condition. A critical temperature specification generally comes from the requirement to avoid a particular wear phenomenon, and this is the basis of a bit design and operating code described in detail in section 9.

Further analysis of the temperature gradients in the cutter assembly has given considerable insight into the thermal stresses that are generated during the transient operating conditions when the bit is beginning to drill and when it is lifted off bottom. For a given cutter geometry, the convective cooling rate is very influential in determining the thermal stresses. In a drilling scenario with the heat input held constant at a value that produces a steady-state wearflat temperature of 700°C, two cooling rates were modeled and compared. These rates represent the typical values; the

heat transfer coefficient for the air-drilling case was h = .01 W/cm ^{2}C and for the water-drilling case it was one hundred times that. Because of the great differences in cooling rate, the temperature regimes within the cutter were qualitatively as well as quantitatively different. The profiles show that the low cooling rate (fig 7.3a) gives high temperatures that are relatively uniform, while the high cooling rate (fig 7.3b) gives lower temperatures with higher gradients near the wearflat. Maximum principal stress distributions for each case are shown in figures 7.4a and 7.4b; the large stress values in the high-rate case are caused by the steep thermal gradient in the wearflat region and in the low-rate case by the differences in thermal expansion coefficients between the diamond and tungsten carbide materials. Both of these effects emphasize the importance of applying weight on the bit slowly, and then holding it as constant as possible.

Finally, the effect of bit balling - the collection of chips and fines around the individual cutters - on the cutter temperatures was investigated. As the cuttings become packed across the bit face they not only impede the bit's advance into the rock, but they shroud the surfaces of the individual cutters and reduce the drilling fluid's ability to cool them. This is particularly important on the diamond surface, because it has at least five times the thermal conductivity of the tungsten carbide. In the model, the effect of a layer of low-conductivity rock flour across the diamond surface is to raise the thermal impedance from the stud to the fluid and to lower the effective heat transfer coefficient for convective cooling. As shown in figure 7.5, a rather thin layer of rock flour can drastically reduce the cooling rate if it is at a relatively high value. This emphasizes the importance of good hydraulics in convective cooling - the fluid must not only have adequate flow to carry the heat away but must keep the cutter clean enough for the heat transfer to be efficient. When specific cutters can be identified as having critical heating or wear problems, it may be necessary to give them individual jets as replacement or augmentation of the conventional nozzles. This is discussed in more detail in sections 8 and 9.

Experimental Measurements -- Part of a contract with General Electric Corporate Research and Development was devoted to measurement of cutting temperatures in a pre-ground PDC cutter/stud assembly. The experimental apparatus was essentially the same as that shown in figure 6.1, but the cutter assembly was fitted with thermocouples in the three locations defined by figure 7.6. The test matrix included two cutting speeds, two rates of penetration, and two coolant flow rates, thus giving eight different test conditions. A complete description of the experiments and results is given in References 15 and 17, but figure 7.7 shows a comparison of the calculated and measured temperatures. Generally, the agreement is very good; the tendency of actual temperatures to be lower than calculated is probably caused by the analytical assumption in these calculations that the friction force is equal to the cutting force (friction force measurements were not available when the calculations were made). Even though the depths of cut are small, this overestimates the friction force and gives a higher calculated temperature. In spite of the slight differences in these results, the experiments were a strong validation of the analytical method.

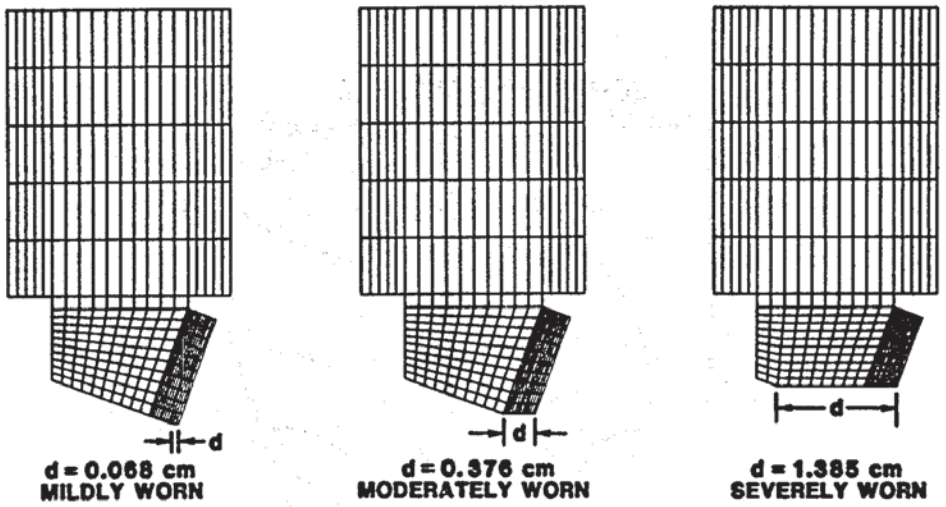

Figure 7.1 -- Finite element meshes for three idealized cutter configurations

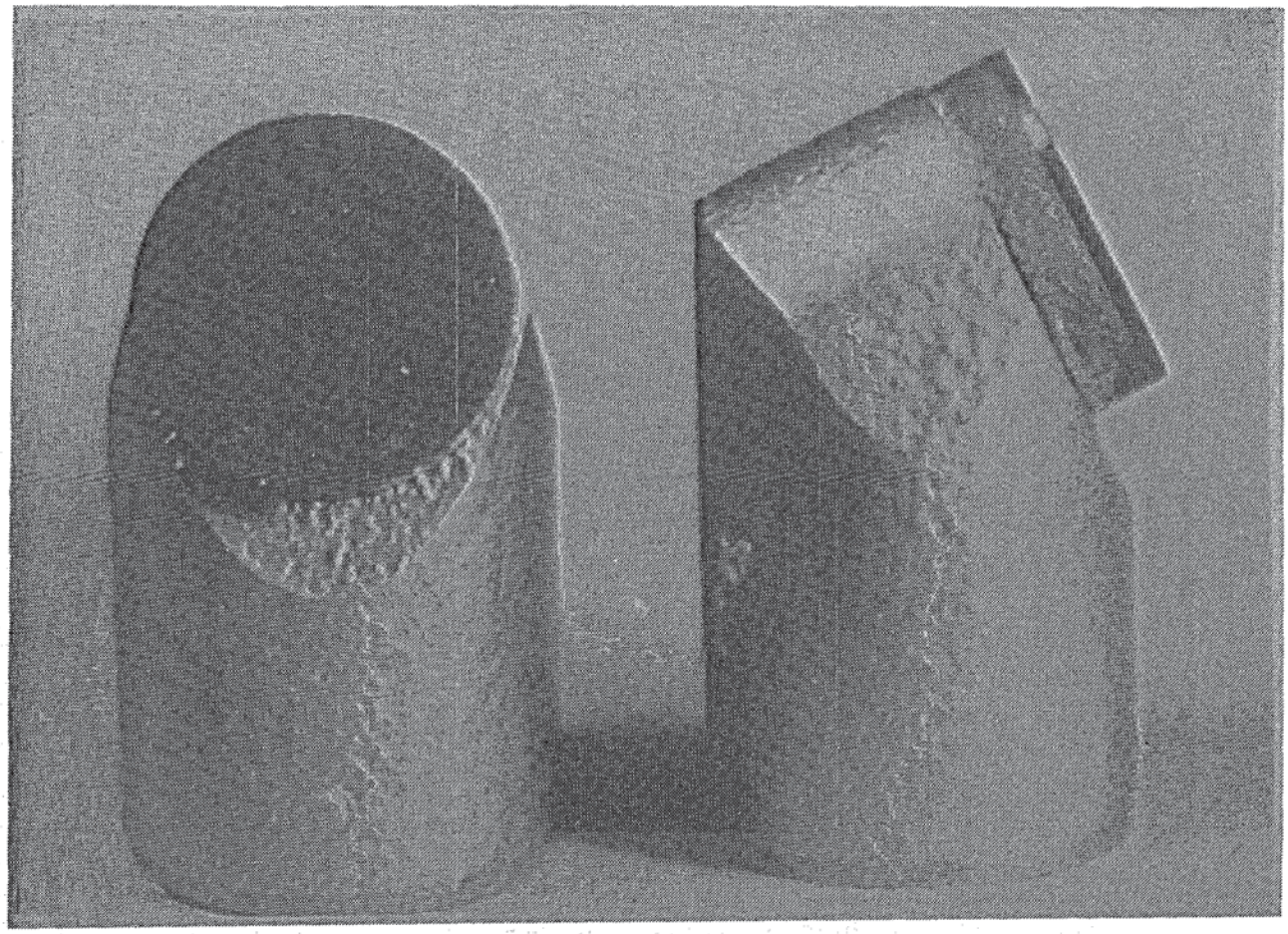

Figure 7.2 -- "Standard" stud-mounted PDC cutter with 0.5 inch diameter compact and 20° backrake

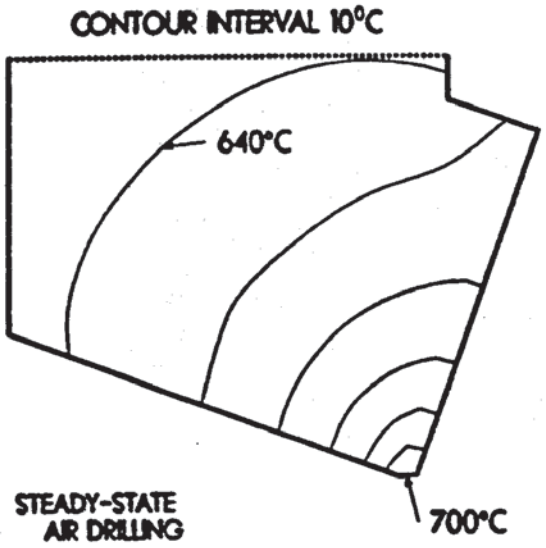

Figure 7.3a -- Isotherms in a frictionally heated cutter with a low convective cooling coefficient

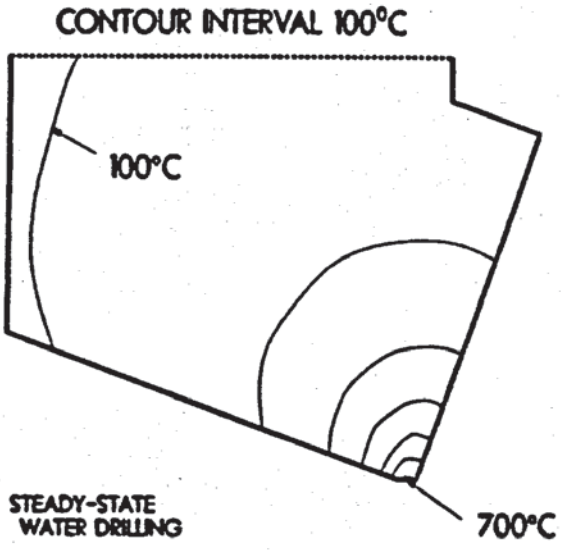

Figure 7.3b -- Isotherms in a frictionally heated cutter with a high convective cooling coefficient

Case	Change From Baseline Analysis	Thermal Response Function, f (°C·cm²/W)											
		Mildly Worn				Moderately Worn				Severely Worn			
		h (W/cm²·°C)				h (W/cm²·°C)				h (W/cm²·°C)			
		0.01	0.10	1.0	5.0	0.01	0.10	1.0	5.0	0.01	0.10	1.0	5.0
1	None	0.956	0.170	0.064	0.035	5.46	0.696	0.325	0.198	23.5	3.22	0.924	0.599
2	Grade 78B WC-Co stud and bit body (k_b = 0.42)	0.988	—	0.066	—	5.68	—	0.370	—	24.5	—	1.34	—
3	Grade 78B WC-Co compact, stud and bit body (k_b = 0.42)	1.02	—	0.078	—	5.86	—	0.495	—	24.6	—	1.52	—
4	Thicker diamond layer (0.140 cm)	0.921	0.151	0.051	0.027	5.31	0.633	0.277	0.160	22.9	3.13	0.878	0.563
5	Cooling of vertical bit body surfaces	0.585	—	0.064	—	3.21	—	0.322	—	12.2	—	0.883	—
6	Internal cooling of cutter	—	—	—	—	5.27	—	0.325	—	—	—	—	—
7	Higher (k_M = 0.05)-and lower (k_M = 0.006) rock thermal conductivity	—	—	—	—	—	—	—	—	—	—	—	—
8	T_s = 50 to 150°C	—	—	—	—	—	—	—	—	—	—	—	—
9	Lower x% of diamond face insulated from fluid:												
	x = 20	0.991	—	0.075	—	5.65	—	0.363	—	24.2	—	0.973	—
	x = 50	1.05	—	0.082	—	5.95	—	0.402	—	25.3	—	1.05	—

Table 7.1 -- Samples of thermal response function for different cutter configurations and cutting conditions

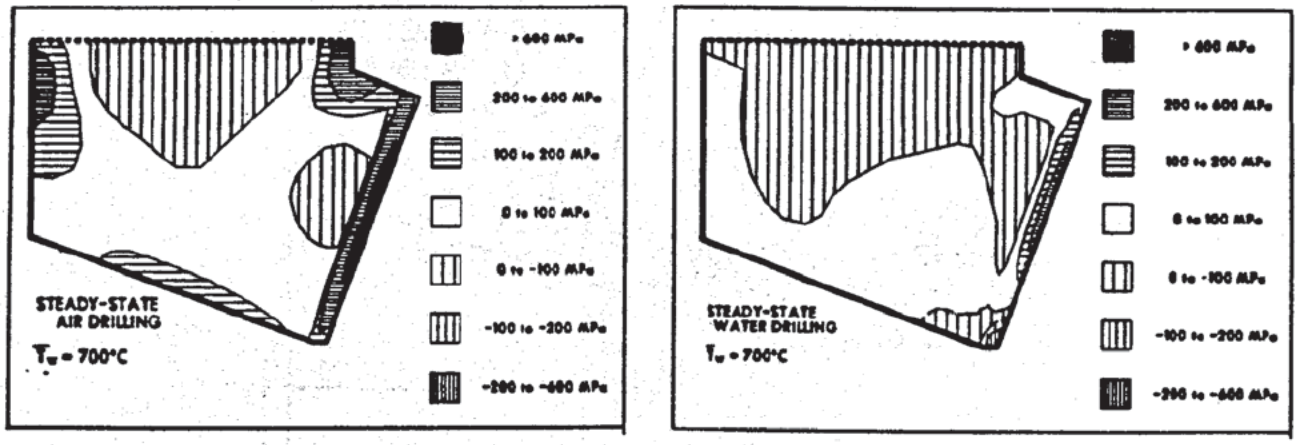

(a) Low cooling rate (b) High cooling rate

Figure 7.4 -- Plastic strain contours in the cutter

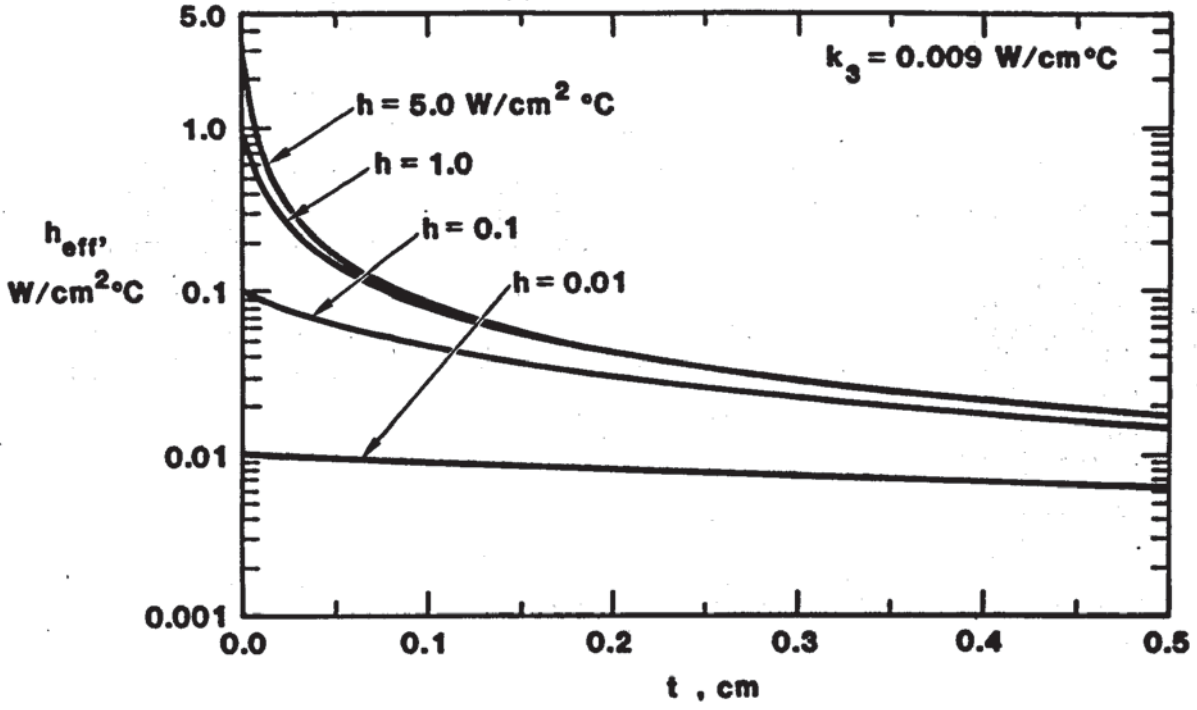

Figure 7.5 -- Effects of bit balling on convective cooling rate (t = thickness of rock flour on cutter)

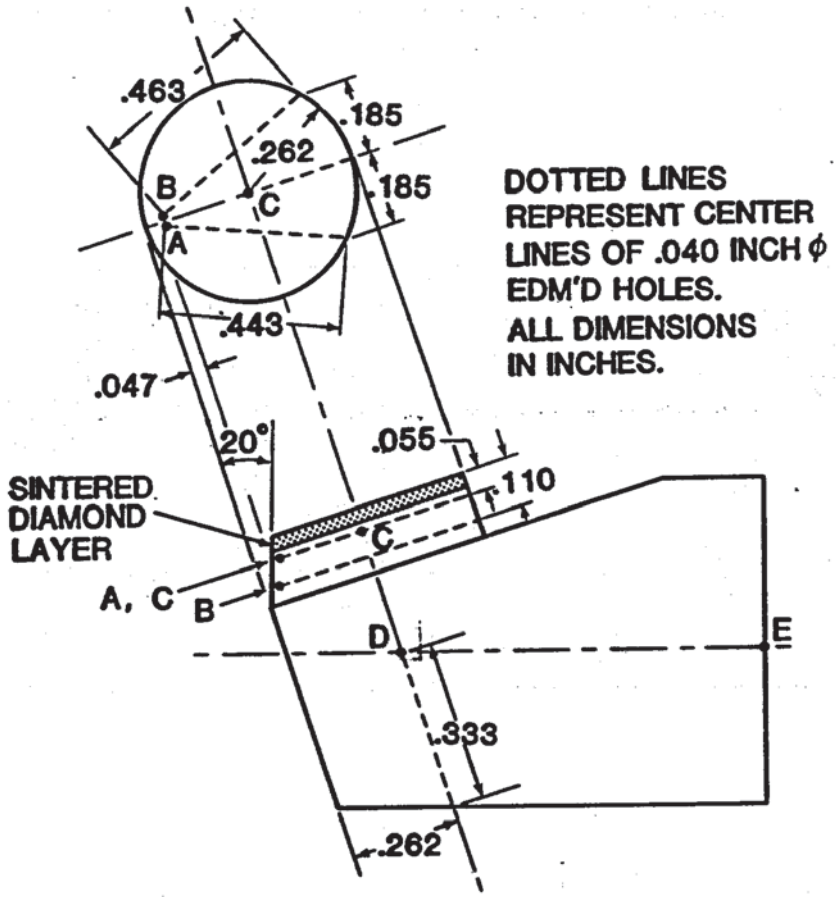

Figure 7.6 -- Thermocouple locations for experimental temperature measurements

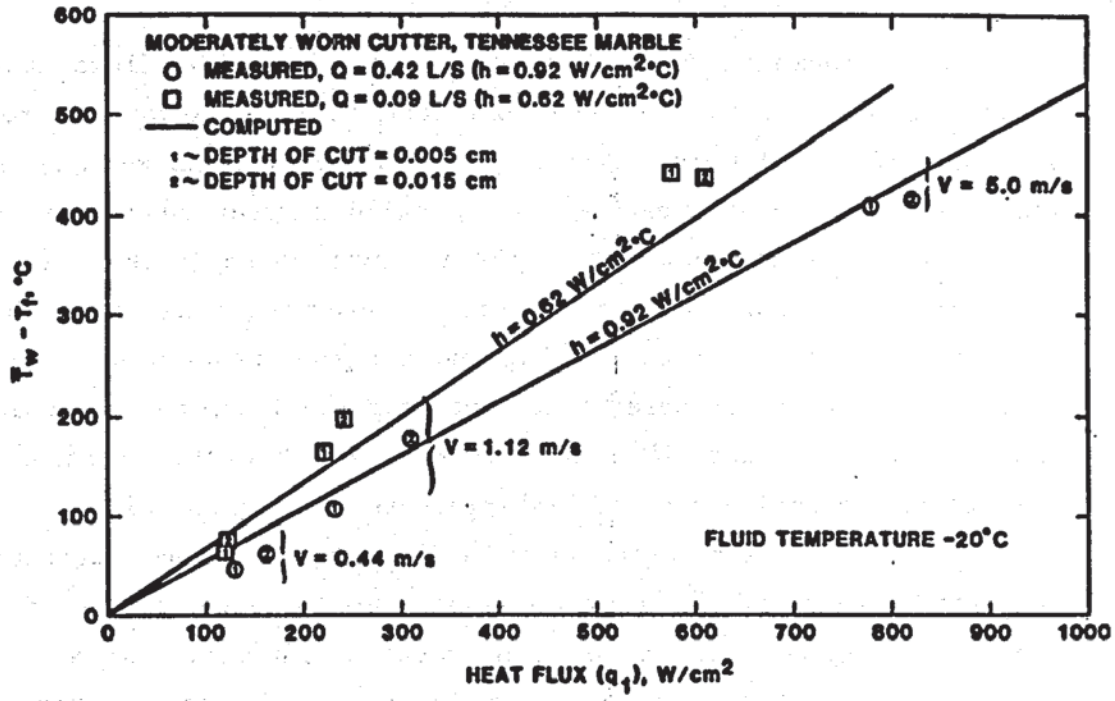

Figure 7.7 -- Comparison of calculated and measured temperatures

8 -- STRUCTURED JETS

The phenomenon of cavitation occurs in those flows where kinetic effects cause the local pressure to drop below the vapor pressure of the liquid, thus creating vapor pockets or bubbles. When these bubbles collapse against a solid surface there are very high impact stresses, well above the strength of any rock. Nozzles that produce cavitating jets are very interesting because of their potential for direct rock cutting and for augmentation of roller-cone bits. Sandia sponsored extensive research into this technology and that work is described in Reference 20, but this section is devoted to the application of high-pressure jets to PDC bits.

There is a distinction between jets which produce cavitation in a rather random fashion and jets which produce "structured" flows that emit regular trains of ring vortices that may or may not cavitate. The tendency of a particular nozzle to cavitate is generally dependent on the nozzle geometry, the fluid velocity, and the static pressure in the nozzle environment. At pressures representative of modest wellbore depths, most nozzles will not cavitate without extreme pump pressures. If the nozzle has a properly designed resonant chamber behind it, however, its flow will always pulsate and will cavitate if the ambient pressure is low enough.

This pulsating flow has been shown to have several beneficial effects on the drilling process:

If the rock is weak enough and the fluid pressure is high enough, the jet will erosively cut the rock directly. This has been demonstrated for several different configurations.

Analysis indicated that as a ring vortex spreads across a given point on the rock surface, the pressure at that point first increases and then decreases to a value lower than the ambient pressure. This means that any loose particles on that point would be lifted, thus improving bottomhole cleaning. This was verified experimentally by directing steady and pulsating jets on an artificial mud cake formed over a filter cloth in a test cell. The pulsating jets proved to be two to four times as effective as steady jets with the same pressure drop in dislodging the mud cake.

Jets directed at the rock in front of drag cutters have been shown by several investigators to reduce the force necessary to cut the rock. Tests done by Sandia at atmospheric pressure showed that cuts with a 2000 psi jet ahead of a PDC cutter reduced cutting forces by 10 to 15%, and a 4500 psi jet reduced them by 50 to 65 percent in Sierra White granite. Based on the force/temperature relation described in the previous section, it is clear that major reductions in force will lower the cutter temperature, thus greatly increasing the ability to drill hard rock.

The importance of this work for PDC bits is centered on the ability of jets to reduce cutter forces. Since there are frequently "critical" cutters which undergo high-temperature, high-wear conditions in a given bit design, the addition of individual jets to these cutters would allow the bit to accept more force (cut harder rock or have higher rate of penetration) and/or have longer life.

Under contract from Sandia, Tracor Hydronautics did most of this work on structured and cavitating jets, and it is reported in detail elsewhere (Ref 21 - 23). A brief summary of the areas that they investigated follows:

Tests of different nozzles' erosivity in different kinds of rock

Design guidelines for nozzles and resonant chambers

Analytic descriptions of the flow fields in the nozzle, in the chamber, in the standoff between the nozzle and the target, and in the vortex spreading across the target

Numerical modeling of the analytic descriptions

Effects of mud on the jet's performance

Direct observation, including photography, of the vortex trains in a flow visualization chamber.

9 -- COMPUTER CODE FOR BIT DESIGN AND OPERATION

The synthesis of much of the preceding work is a code that calculates forces, temperatures, and wear rates of individual cutters in a user-defined bit design. These values are then integrated over the bit face to give total weight-on-bit, torque, and side load. This information is very useful, for it not only identifies critical cutters in a proposed bit design, but it defines an operating envelope for an existing bit.

The most desirable design criterion for a PDC bit is that all of the individual cutters wear at the same rate. If a bit has certain "critical" cutters with much higher temperatures or wear rates than others, the design can be changed by adding jet augmentation to the critical cutters or by increasing the cutter density at the critical radius. Either of these modifications will lower the wear rate at the critical points and make the total bit wear more uniform.

Cutting a given rock with a cutter in a given condition (sharp, mildly worn, etc.) requires a characteristic penetrating stress under the cutter wearflat, thus defining the force on that cutter. A scenario of drilling a specific rock with a specific bit can then be analyzed by using the characteristic penetrating stress for each cutter, applying the associated forces in the proper directions, and summing all forces. Furthermore, this summation can be iterated over time, because the code calculates the increasing wearflat areas and forces as the bit drills ahead. This output can be used to create an operating envelope bounded by the minimum WOB required to drill the given rock and the maximum WOB/rotary speed combination to avoid critical temperatures. The code also gives the torque, side load, and bending moment on the bit; the rate of penetration; and the wear of each cutter. As the drilling calculation proceeds, the wear rate of each cutter is tracked and the drilling conditions are updated with the new force data. Reference 24 is a detailed description, including program listing, of the PDCWEAR code, but in the following narrative we will

summarize the principles that underlie the code's derivation and operation.

Analysis

To assemble the PDCWEAR code, it is necessary to have analytical and/or empirical descriptions of several elements of the bit's behavior. These components include the following:

A relation for single cutters between forces and depth of cut

The effect of overlapping cutter paths

A relation between the cutter's wear rate and the cutting conditions

An equation to give the cutter's wearflat temperature

The components were derived in the ways described below.

Force/depth of cut relation:

The most important variables in a cutting force model are the rock type, the depth of cut, and the cutter condition (sharp, mildly worn, etc.). Since it was clear that worn cutters required more force, the penetrating force (F, normal to the direction of cut) was converted to a stress by dividing by the wearflat area (A_w) and this stress (S) was plotted against depth of cut (d) (figs 9.1 and 9.2). The data all fall on a curve that is of the form

$$F/A_w = S = C_1 d^{n1} \qquad (1)$$

where C_1 and n1 are constants determined by curve fitting. Apparently these constants, for a given rock and given operating conditions, do not change as the wearflat grows. This means that penetrating stress is constant for a given depth of cut (with a cutter having measurable wearflat area) and this holds true even if the cutter size changes. Thus, a large cutter with the same wearflat area as a small cutter will require the same force, but will remove more rock and be more efficient. For new cutters with wearflat area essentially zero, the correlation coefficients are associated with a force equation (see fig 9.3)

$$F = C_2 d^{n2}. \qquad (2)$$

Experimental data have also shown that, for hard rocks such as granite, the threshold penetrating stress is on the order of the compressive strength of the rock, but for softer rocks such as sandstone, the cutter can penetrate at stresses considerably less than the rock's compressive strength. In the hard rocks, the cutter may act as a moving indentor, removing the rock by crushing and tensile fracture, while the shearing action is more important in the softer rocks.

Once the relation between the penetrating force and the depth of cut is established, it is still necessary to estimate the force in the direction of the cut. For a given combination of rock and cutting conditions, the ratio of the drag force F_d to the penetrating force F is relatively constant with changes in depth of cut and wearflat area. That is, $F_d = u_d F$, where u_d is defined as the drag coefficient. Examples of drag coefficient data are shown in figures 9.4 and 9.5.

The forces on a single cutter are now completely described with the exception of the case in which a fluid jet impinges on the rock ahead of the cutter. Cutter forces with waterjets of 80, 2000, and 4500 psi directed on the rock ahead of the cutter are shown in figure 9.6, where it is clear that the higher pressure jets significantly reduce the forces. This reduction is apparently the result of better cutter cleaning, where the absence of fines allows a higher stress concentration at the cutter tip, and actual rock damage with the 4500 psi jet, which reduces the cross-sectional area and rock strength ahead of the cutter. Even though the absolute value of the forces can change drastically, the drag coefficient is not greatly affected -- it is generally reduced by the same value as the reduction in friction coefficient between the rock and cutter due to liquid lubrication.

Effect of overlapping cutter paths:

Any bit which is to cover the bottomhole area must have overlapping or interacting cutter paths. If we are to integrate the individual cutter forces to get whole-bit loads, then we must know the effect of these interactions.

Considering an arbitrary cutter, such as that in figure 9.7, we can project the profile of the rock that it cuts on the cutter face as shown. Then, using the fact that drag coefficient does not vary greatly with depth of cut, we can define an equivalent depth of cut for a single cutter that would impose the same loads on it as the forces on the arbitrary cutter in the actual interacting cut. The depth of the equivalent cut, δ_e, is taken to be the mean height of the actual cut profile. The experimental and calculated stresses for equivalent depths of interacting cuts are compared in figure 9.8 and show good agreement.

Wear rate/cutting condition correlation:

The behavior of the wear rate in the model is important for several reasons:

The basic goal of the bit's design is for all cutters to wear at the same rate.

Wear rate increases by one to two orders of magnitude when wear flat temperatures exceed 350°C (see section 6).

The wear rate controls the growth of the wearflat, and thus the forces on the cutter.

The general theory of abrasive wear indicates that for a given cutter on a bit with constant penetration rate, the volume of material worn from that cutter is proportional to its path length. Assumption of constant penetration rate also implies an increasing weight on bit to maintain the penetrating stress as the wearflat area grows. The wear volume, V_w, is then related to the length of hole drilled, l_h, by the equation: $dV_w/dl_h = -(2Fx_cC_aN)/ROP$, where:

F - penetrating force

x_c - cutter radius from center of bit

C_a - abrasive wear constant determined by abrasiveness of rock and wear resistance of cutter material

N - bit rotary speed

ROP - bit's rate of penetration.

This equation applies to the regime in which thermally accelerated wear (wearflat temperature above 350°C) does not occur.

Although the wear equation gives the volume of cutter material removed, this is an inconvenient quantity to measure. The length of the wearflat, L, is much more easily measured and for the "standard" cutter geometry considered here (stud-mounted, 20° back rake) can be related to the wear volume by $L = 2.4\ V_w^{0.4}$.

Finally, in considering the performance of a bit, it is needlessly complicated to use the wear volume algorithm for each cutter if the wears can be expressed in terms of a reference cutter. If cutter 1 is defined as the cutter nearest the center of the bit, then a wear ratio, WR, can be used to give the wear rate of any other cutter relative to number one. The wear ratio for the "i"th cutter is $WR = (Fx_c)_i/(Fx_c)_1$. The topic of cutter wear (including differences in wearflat geometry between hard-rock and soft-rock wear mode) is treated extensively in References 24 and 25, but this is a synopsis of the key wear calculation elements in the code.

Wearflat temperatures:

Calculation of wearflat temperatures is discussed in section 7, and in more detail in References 17 - 19. Without repeating the equations or derivations, we will simply state that the most important consequence of being able to calculate wearflat temperatures is the identification of drilling conditions that produce a critical stress on the cutter. Critical stress is defined as the stress which generates a wearflat temperature above 350°C, and thus a greatly increased wear rate. By using this criterion to limit weight-on-bit for various rates of penetration and rotary speeds, we can develop an operating envelope for specific bit/rock combinations.

Code development

These four elements are assembled into a modified version of the code STRATAPAX, called PDCWEAR. STRATAPAX was originally developed to calculate cutter placement on a bit and was published by Sandia in 1982 (Ref 26). It used the criterion of equalizing either the volume or the cross-sectional area swept by each cutter to specify cutter locations in an arbitrary bit design. The

algorithms that calculate cut volumes and cross-sections in STRATAPAX were extensively modified to include the wear, force, and temperature calculations of the new code. PDCWEAR, developed on a VAX 8650 computer, is written in Fortran 77, which complies with the ANSI standard.

Sample calculations

To illustrate the inputs that are required and the outputs that are generated, a brief outline of a sample problem appears below. This is the same problem that is described in considerably more detail in the PDCWEAR Users' Manual (Ref 24). The analysis is based on the 8.5-inch diameter, 21 cutter bit shown in figure 9.9. Required input data fall into three categories and are entered into these three corresponding input files:

Bit Design Data (file BITDES.DAT)
- Three dimensional specification of position and orientation for each cutter.
- Compact radius of each cutter.
- Backrake angle of each cutter.
- Convective cooling coefficient.
- Type of cutter (with or without waterjet assistance).

Initial Cutter Wear State (file WEARCF.DAT)
- Wearflat length of each cutter.
- Wearflat width of each cutter.
- Wearflat area of each cutter.
  [All these values can be specified zero for a new bit.]

Operating Conditions (file OPCOND.DAT)
- Thermal conductivity of the rock.
- Thermal diffusivity of the rock.
- Friction coefficient between cutter and rock.
- Drag coefficients for sharp and worn cutters.
- Correlation constants and exponents for sharp and worn cutters with and without waterjets (equations 1 and 2).
- Abrasive wear constant for cutter material/rock combination.
- Bit rotary speed.
- Drilling fluid temperature.
- Rates of penetration; at least three required.

Once the input data have been collected and entered in the proper files, the program is run interactively with the user specifying which input files are to be used in the analysis. Output

gives detailed information about each cutter, as well as integrated values for the whole bit. These data, based on the originally specified cutter wear conditions, are available for each specified penetration rate (as shown in Tables 9.1 and 9.2). These are, however, instantaneous values and do not explicitly show how the wear progresses as the bit drills ahead.

For further iteration, the user must choose a wear mode (hard-rock or soft-rock) and a new, larger wearflat area for the cutter with the largest wearflat at that time. If the bit begins the run with all sharp cutters (wearflats zero), the outermost cutter is chosen as the reference. Once these new conditions have been inserted, the program repeats the calculations of bit and cutter performance, but also gives the length of hole drilled to achieve the new wearflat area (Table 9.3). This process can be repeated until cutters are so badly worn that the governing equations are no longer valid.

The tabulated results can also be plotted in a great variety of ways. If we define certain values of the largest wearflat's area as being "worn" or "worn out" (e.g., worn = 0.040 in^2, worn out = 0.10 in^2), then a graphical presentation (figures 9.10 - 9.12) is effective in showing the bit's performance.

General conclusions from the bit analysis

A number of conclusions about bit and cutter behavior can be inferred from the analysis in this code. Some of these have been given, others not discussed above are given below:

Over the experimental range of cutter sizes, penetrating forces are independent of the cutter diameter -- meaning that larger cutters are more efficient.

There are two distinct cutter wear modes. Soft rocks wear the flat at an angle to the rock surface, keeping the contact area smaller and the cutter sharper. Hard rocks produce wearflats that are more nearly parallel with the rock surface, compounding the tendency for these rocks to require more force.

Certain cutter placements can produce significant side forces and bending moments on a bit, enhancing the chances for bit wobble, overgage hole, and hole deviation.

Bit profile can significantly affect performance and wear. Sharper profiles initially require less weight-on-bit, but they wear faster and eventually require more WOB.

Increased rotary speed degrades the bit life, even at constant rate of penetration. If ROP must be improved, it is better to increase weight on bit than rotary speed.

In summary, the PDCWEAR program is a tool that can be used to compare bit designs, to gain detailed information on individual cutters so that a bit design is optimum, and to predict performance of a specific bit/rock combination.

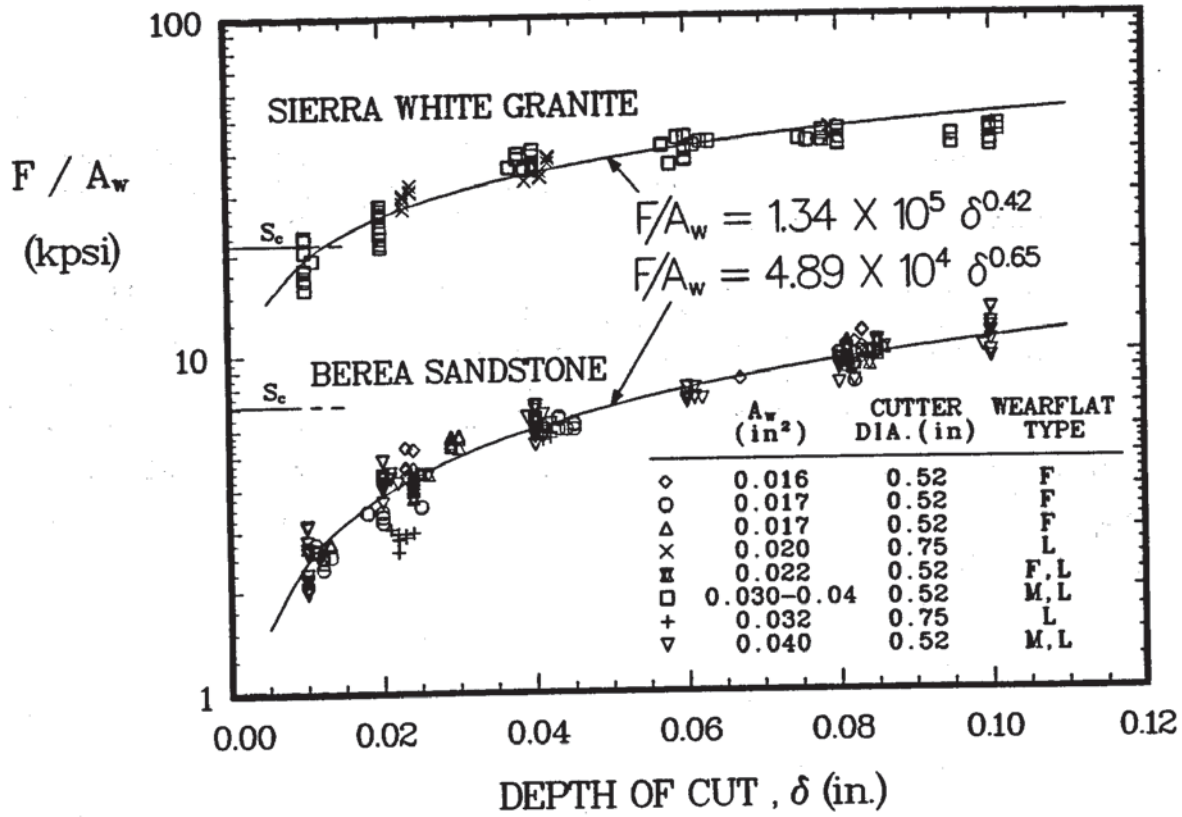

Figure 9.1 -- Variation of penetrating stress with depth of cut (Wearflats are: F - field worn, L - lab worn, M - machine ground)

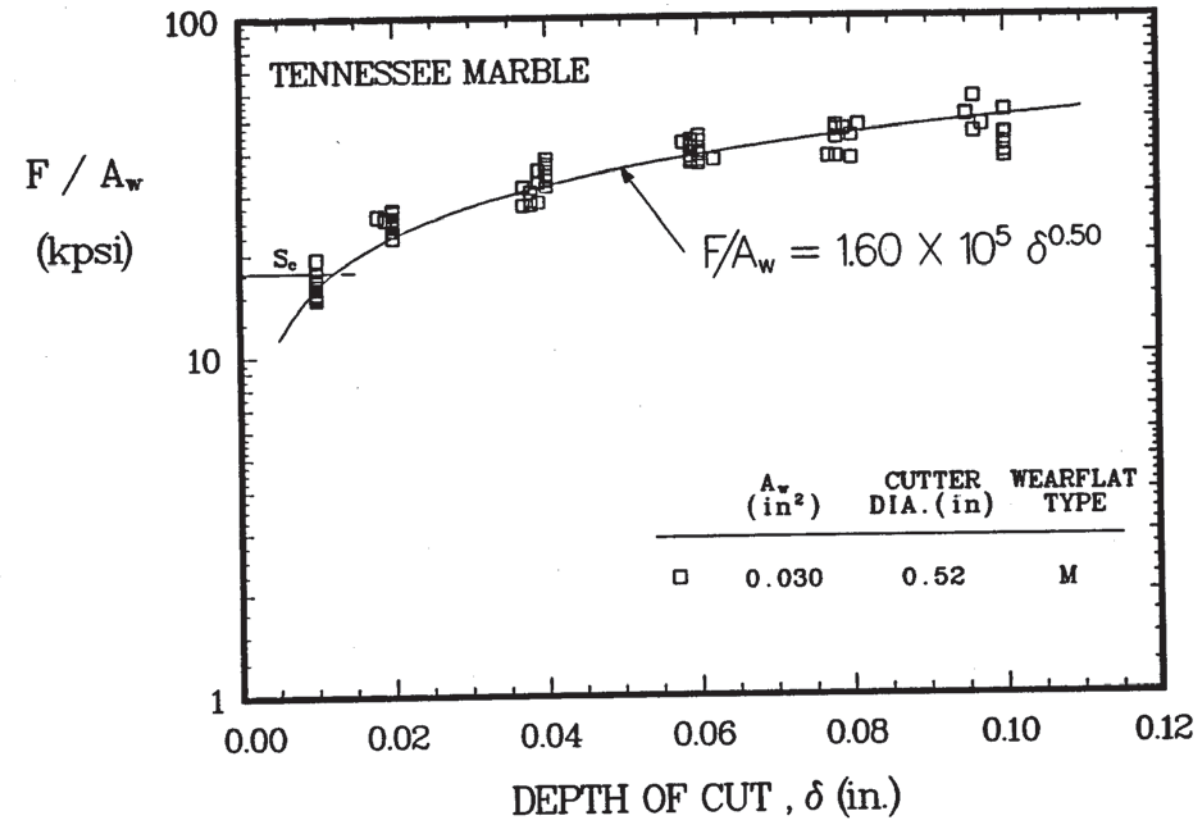

Figure 9.2 -- Variation of penetrating stress with depth of cut

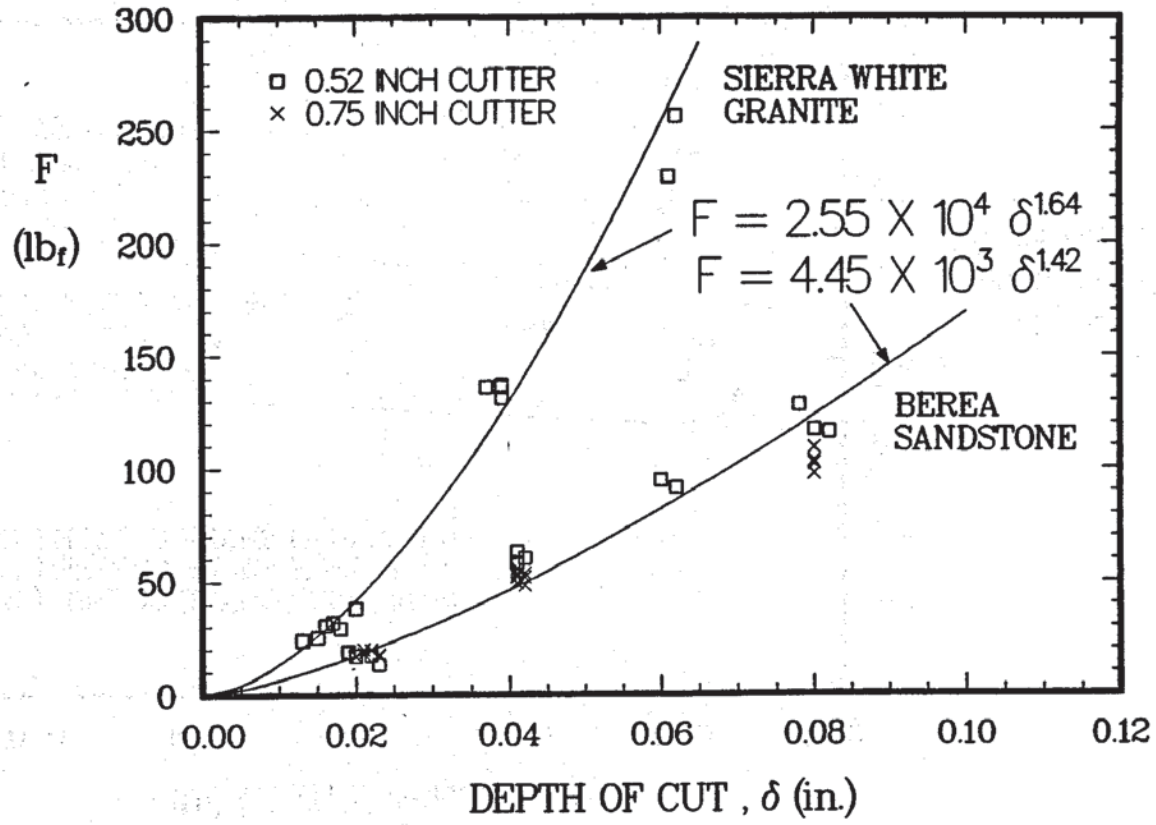

Figure 9.3 -- Variation of penetrating force with depth of cut (sharp cutters)

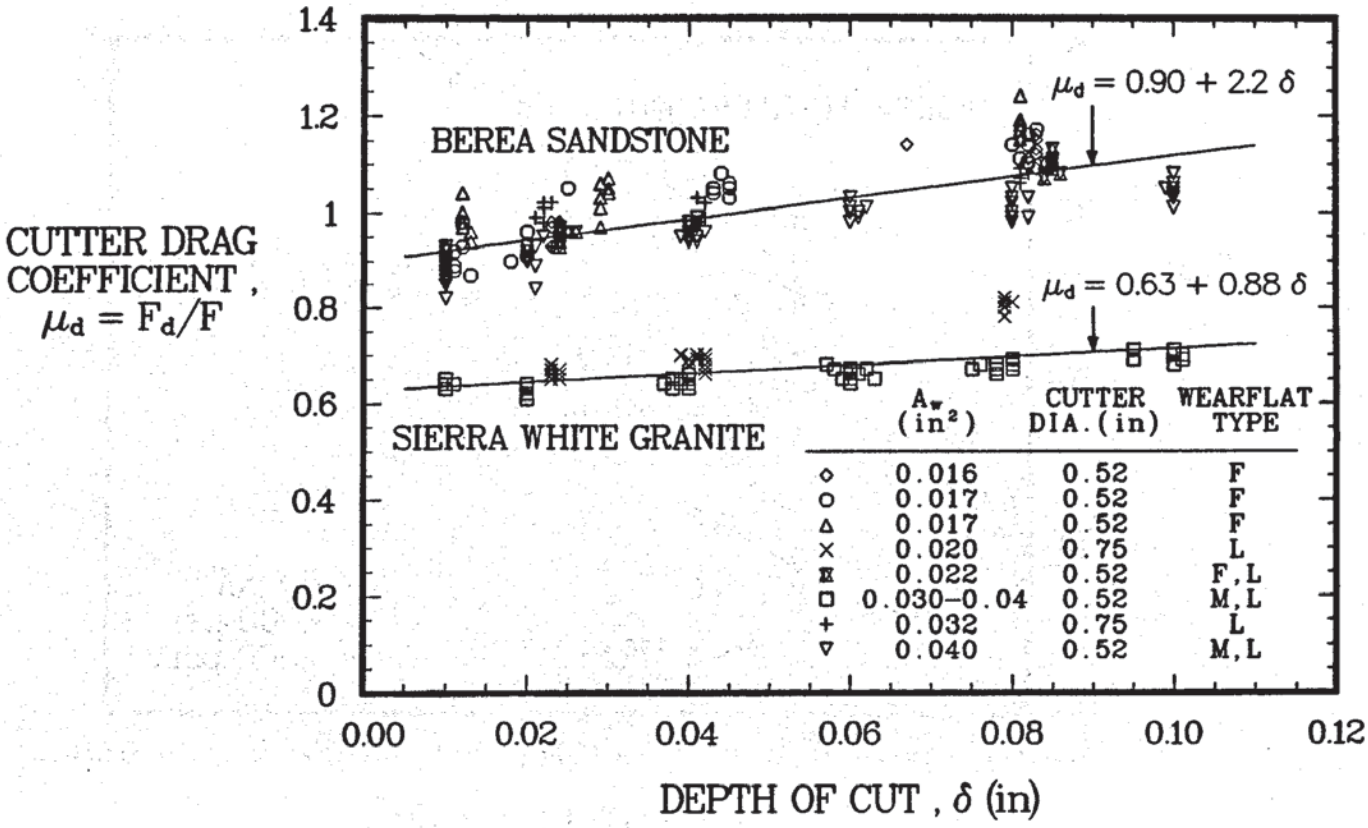

Figure 9.4 -- Variation of drag coefficient with depth of cut

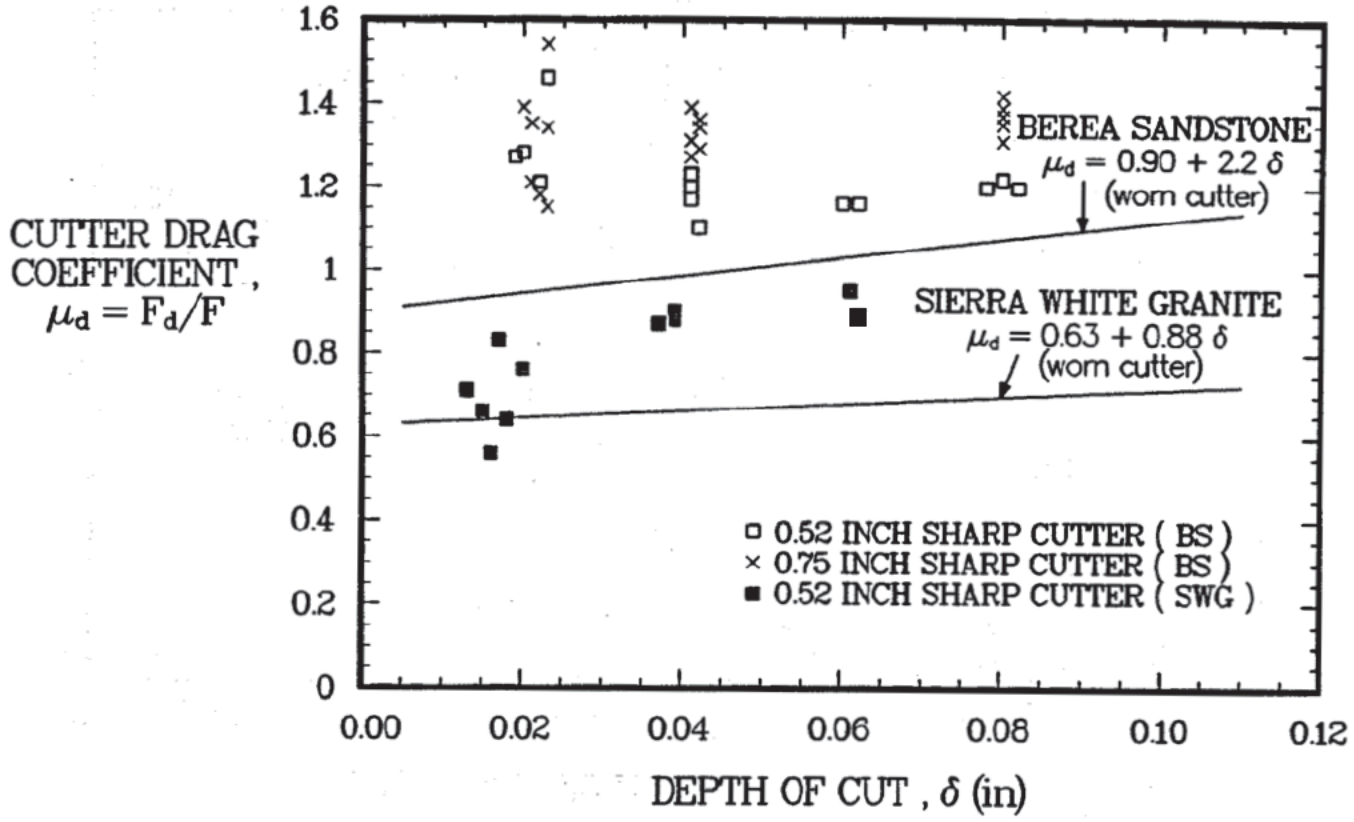

Figure 9.5 -- Variation of drag coefficient with depth of cut (sharp cutters)

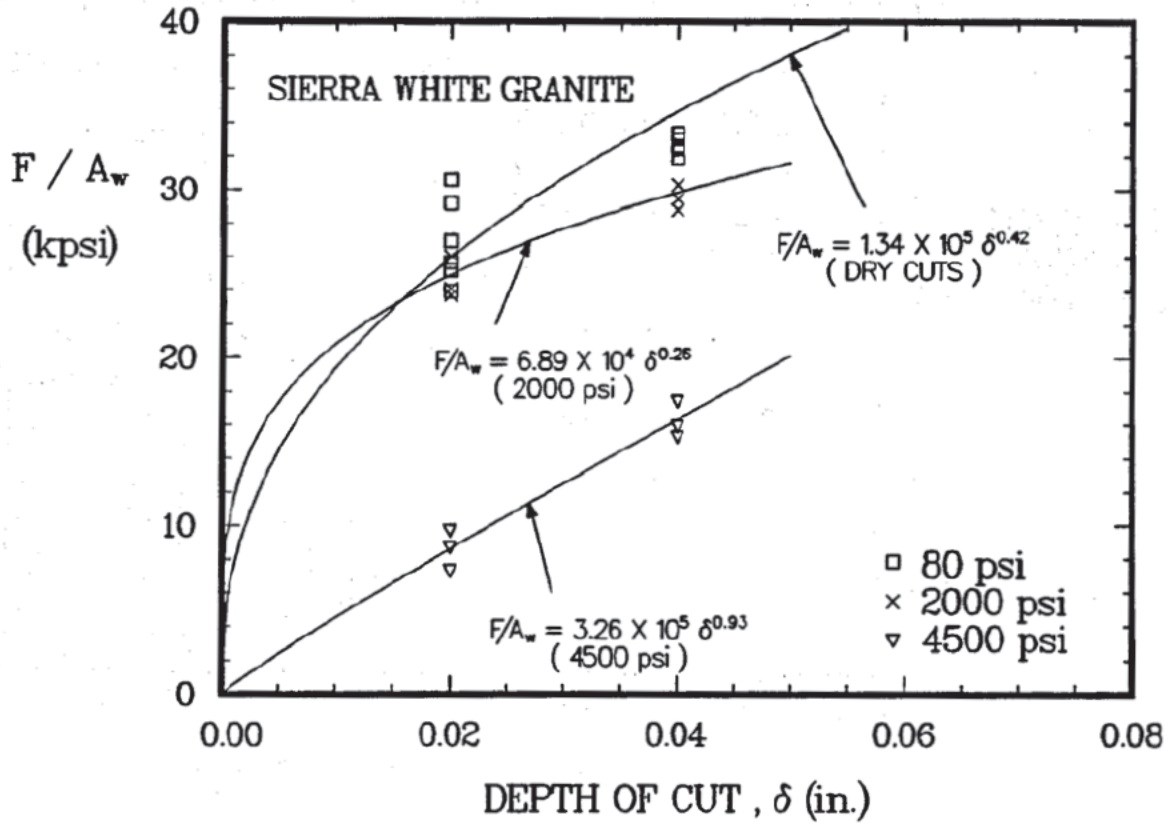

Figure 9.6 -- Effect of waterjet assistance on penetrating stress

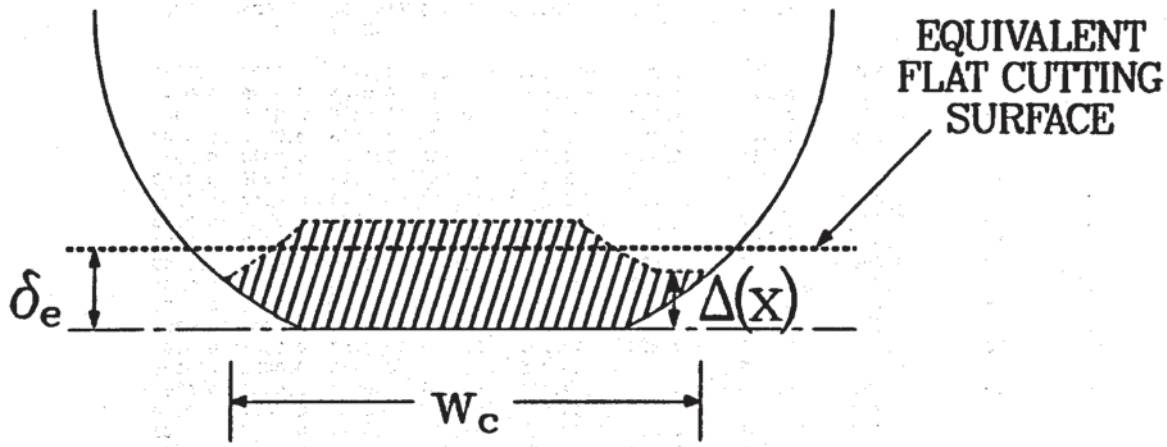

Figure 9.7 -- Projection of actual cut rock profile on the face of an arbitrary cutter

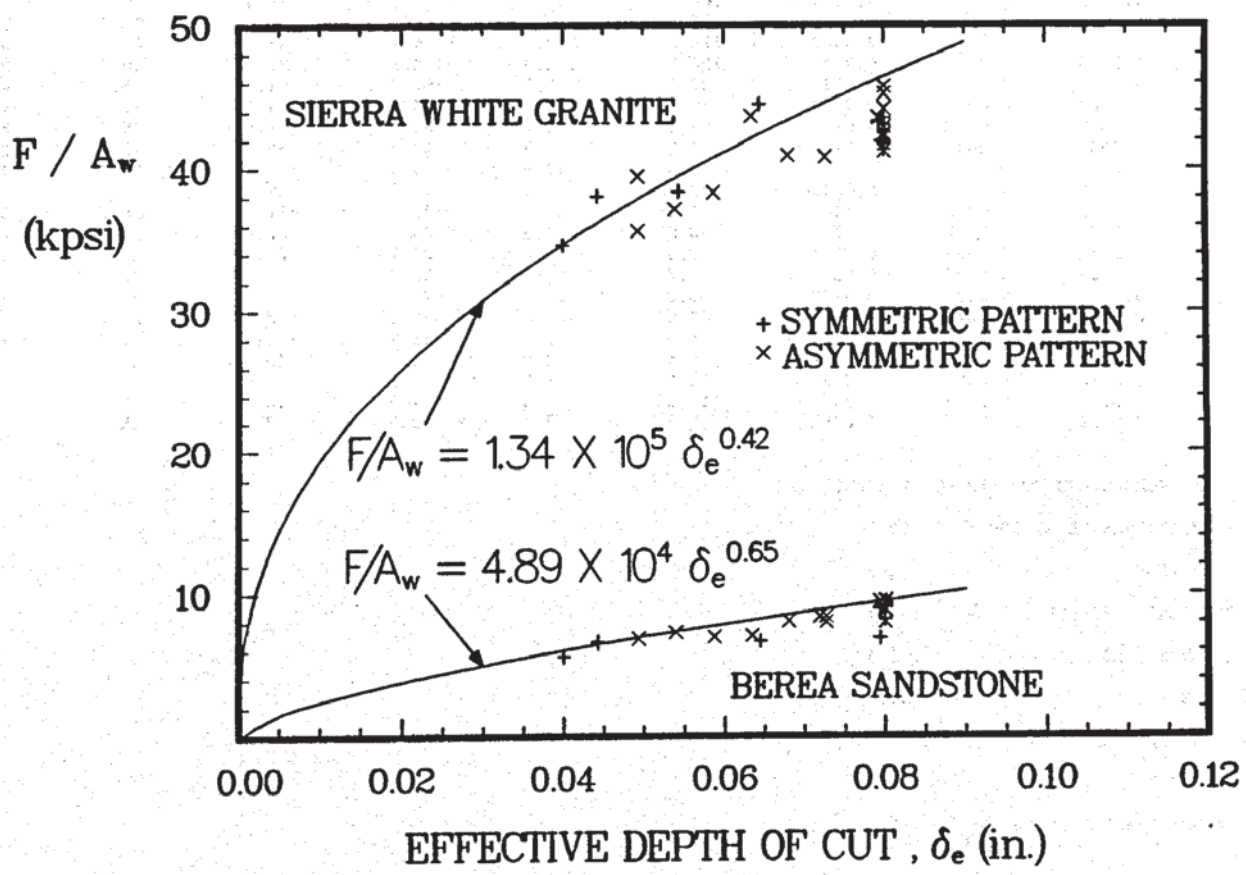

Figure 9.8 -- Comparison of predicted and measured penetrating stresses for interacting cuts

CUTTER	CUTTING ORDER	CUTTING HEIGHT (IN.)	WEARFLAT LOCATION XBC (IN.)	WEARFLAT LOCATION ZBC (IN.)	CUTTER INCL. ANGLE (DEG.)	CUTTER WEAR ANGLE (DEG.)	VOLUME OF CUT (IN**3/ REV)	AREA OF CUT (IN**2)	EFFECTIVE DEPTH OF CUT (IN.)
1	20	0.645	0.205	0.967	-15.000	-23.149	0.0153	0.0099	0.0521
2	8	0.768	0.694	1.104	-10.000	-16.660	0.0405	0.0090	0.0447
3	14	0.909	1.116	1.237	-5.000	-20.358	0.0558	0.0078	0.0390
4	18	1.018	1.544	1.366	-2.000	-8.296	0.0873	0.0089	0.0437
5	4	1.004	1.954	1.357	0.000	0.609	0.0856	0.0070	0.0336
6	11	1.011	2.276	1.363	2.000	-3.241	0.0823	0.0058	0.0290
7	21	1.010	2.525	1.361	5.000	4.965	0.0658	0.0042	0.0232
8	6	0.977	2.707	1.322	10.000	11.550	0.0551	0.0032	0.0198
9	13	0.953	2.869	1.293	15.000	15.392	0.0578	0.0032	0.0197
10	2	0.900	3.036	1.231	20.000	20.014	0.0645	0.0034	0.0203
11	9	0.853	3.204	1.172	25.000	24.940	0.0665	0.0033	0.0200
12	16	0.792	3.366	1.100	30.000	29.108	0.0672	0.0032	0.0195
13	3	0.698	3.531	0.990	35.000	34.019	0.0742	0.0034	0.0201
14	10	0.605	3.700	0.876	40.000	38.773	0.0757	0.0033	0.0197
15	17	0.490	3.866	0.738	45.000	45.281	0.0775	0.0032	0.0195
16	19	0.366	4.005	0.592	47.500	49.702	0.0637	0.0025	0.0167
17	5	0.228	4.123	0.431	50.000	54.162	0.0559	0.0022	0.0150
18	12	0.116	4.213	0.305	52.500	57.064	0.0412	0.0016	0.0122
19	1	0.001	4.304	0.131	55.000	67.023	0.0162	0.0006	0.0087
20	7	0.008	4.302	0.143	55.000	66.192	0.0174	0.0006	0.0093
21	15	0.015	4.306	0.138	55.000	67.883	0.0152	0.0006	0.0081

ROCK-DEPENDENT RESULTS FOR PENETRATION RATE = 10.00 FT/HR

CUTTER	VOLUME OF CUT (IN**3/REV)	AREA OF CUT (IN**2)	EFFECTIVE DEPTH OF CUT (IN.)	PENETRATING FORCE (LBF)	DRAG FORCE (LBF)	VERTICAL FORCE (LBF)	RADIAL FORCE (LBF)	WEARFLAT TEMPERATURE (DEG. C)	WEAR RATIO
1	0.0153	0.0099	0.0521	200.6	150.5	-184.5	78.9	26.7	1.00
2	0.0405	0.0090	0.0447	155.8	116.9	-149.3	44.7	26.7	2.62
3	0.0558	0.0078	0.0390	124.5	93.4	-116.7	43.3	26.7	3.37
4	0.0873	0.0089	0.0437	150.3	112.8	-148.8	21.7	26.7	5.64
5	0.0856	0.0070	0.0336	97.8	73.3	-97.8	-1.0	26.7	4.64
6	0.0823	0.0058	0.0290	76.8	57.6	-76.7	4.3	26.7	4.25
7	0.0658	0.0042	0.0232	53.2	39.9	-53.0	-4.6	26.7	3.26
8	0.0551	0.0032	0.0198	41.1	30.8	-40.3	-8.2	26.7	2.70
9	0.0578	0.0032	0.0197	40.8	30.6	-39.4	-10.8	26.7	2.84
10	0.0645	0.0034	0.0203	42.7	32.1	-40.2	-14.6	26.7	3.15
11	0.0665	0.0033	0.0200	41.8	31.3	-37.9	-17.6	26.7	3.25
12	0.0672	0.0032	0.0195	39.9	29.9	-34.9	-19.4	26.7	3.26
13	0.0742	0.0034	0.0201	41.8	31.4	-34.7	-23.4	26.7	3.59
14	0.0757	0.0033	0.0197	40.7	30.5	-31.3	-26.0	26.7	3.66
15	0.0775	0.0032	0.0195	39.9	29.9	-28.1	-28.4	26.7	3.75
16	0.0637	0.0025	0.0167	30.9	23.2	-20.0	-23.6	26.7	3.00
17	0.0559	0.0022	0.0150	25.9	19.4	-15.2	-21.0	26.7	2.59
18	0.0412	0.0016	0.0122	18.5	13.9	-10.1	-15.5	26.7	1.89
19	0.0162	0.0006	0.0087	10.6	8.0	-4.1	-9.8	26.7	1.11
20	0.0174	0.0006	0.0093	11.9	8.9	-4.8	-10.9	26.7	1.24
21	0.0152	0.0006	0.0081	9.5	7.1	-3.6	-8.8	26.7	0.99

INTEGRATED FORCES AND MOMENTS FOR THE FULL BIT:

SIERRA WHITE GRANITE AT ROP = 10.0

TOTAL WOB (LBF) = 1171.1

DRILLING TORQ. (FT-LBF) = 159.1

X SIDE FORCE (LBF) = 1.4

Y SIDE FORCE (LBF) = -109.0

RESULTANT SIDE FORCE (LBF) = 109.0

B. M. ABOUT X-AXIS (FT-LBF) = 15.3

B. M. ABOUT Y-AXIS (FT-LBF) = -1.2

Table 9.1 -- Sample output for penetration rate = 10 feet/hour

CUTTER	CUTTING ORDER	CUTTING HEIGHT (IN.)	WEARFLAT LOCATION XBC (IN.)	WEARFLAT LOCATION ZBC (IN.)	CUTTER INCL. ANGLE (DEG.)	CUTTER WEAR ANGLE (DEG.)	VOLUME OF CUT (IN**3/ REV)	AREA OF CUT (IN**2)	EFFECTIVE DEPTH OF CUT (IN.)
1	20	0.705	0.217	1.032	-15.000	-21.355	0.0624	0.0399	0.1075
2	8	0.792	0.698	1.130	-10.000	-16.084	0.1646	0.0362	0.1004
3	14	0.951	1.128	1.283	-5.000	-18.456	0.2314	0.0320	0.0927
4	18	1.070	1.563	1.421	-2.000	-5.535	0.3462	0.0351	0.0983
5	4	1.017	1.966	1.369	0.000	2.288	0.3440	0.0279	0.0852
6	11	1.043	2.296	1.396	2.000	-0.304	0.3244	0.0226	0.0740
7	21	1.070	2.541	1.419	5.000	7.267	0.2863	0.0180	0.0628
8	6	0.997	2.716	1.340	10.000	12.966	0.2177	0.0127	0.0497
9	13	0.993	2.883	1.329	15.000	17.469	0.2116	0.0117	0.0467
10	2	0.907	3.044	1.235	20.000	21.340	0.2781	0.0146	0.0540
11	9	0.880	3.220	1.191	25.000	27.626	0.2631	0.0130	0.0503
12	16	0.838	3.377	1.140	30.000	30.948	0.2522	0.0119	0.0476
13	3	0.710	3.541	0.996	35.000	35.647	0.3073	0.0139	0.0524
14	10	0.636	3.711	0.898	40.000	41.895	0.2992	0.0129	0.0503
15	17	0.542	3.880	0.775	45.000	48.259	0.3282	0.0135	0.0518
16	19	0.423	4.023	0.626	47.500	53.909	0.2319	0.0092	0.0407
17	5	0.244	4.128	0.440	50.000	55.507	0.2216	0.0086	0.0385
18	12	0.153	4.211	0.345	52.500	56.502	0.1093	0.0041	0.0238
19	1	0.006	4.293	0.159	55.000	63.107	0.0795	0.0030	0.0192
20	7	0.032	4.287	0.197	55.000	61.325	0.1040	0.0039	0.0228
21	15	0.059	4.304	0.188	55.000	67.023	0.0600	0.0022	0.0154

ROCK-DEPENDENT RESULTS FOR PENETRATION RATE = 40.00 FT/HR

CUTTER	VOLUME OF CUT (IN**3/REV)	AREA OF CUT (IN**2)	EFFECTIVE DEPTH OF CUT (IN.)	PENETRATING FORCE (LBF)	DRAG FORCE (LBF)	VERTICAL FORCE (LBF)	RADIAL FORCE (LBF)	WEARFLAT TEMPERATURE (DEG. C)	WEAR RATIO
1	0.0624	0.0399	0.1075	657.7	493.3	-612.6	239.5	26.7	1.00
2	0.1646	0.0362	0.1004	587.8	440.9	-564.8	162.9	26.7	2.88
3	0.2314	0.0320	0.0927	515.4	386.6	-488.9	163.2	26.7	4.08
4	0.3462	0.0351	0.0983	567.5	425.6	-564.9	54.7	26.7	6.22
5	0.3440	0.0279	0.0852	448.9	336.7	-448.5	-17.9	26.7	6.19
6	0.3244	0.0226	0.0740	356.7	267.5	-356.7	1.9	26.7	5.74
7	0.2863	0.0180	0.0628	272.5	204.4	-270.3	-34.5	26.7	4.86
8	0.2177	0.0127	0.0497	185.6	139.2	-180.9	-41.6	26.7	3.54
9	0.2116	0.0117	0.0467	167.4	125.6	-159.7	-50.3	26.7	3.39
10	0.2781	0.0146	0.0540	212.4	159.3	-197.9	-77.3	26.7	4.54
11	0.2631	0.0130	0.0503	189.0	141.8	-167.5	-87.7	26.7	4.27
12	0.2522	0.0119	0.0476	172.9	129.7	-148.3	-88.9	26.7	4.10
13	0.3073	0.0139	0.0524	202.6	152.0	-164.7	-118.1	26.7	5.03
14	0.2992	0.0129	0.0503	189.1	141.8	-140.7	-126.3	26.7	4.92
15	0.3282	0.0135	0.0518	198.3	148.7	-132.0	-148.0	26.7	5.40
16	0.2319	0.0092	0.0407	133.5	100.1	-78.6	-107.9	26.7	3.77
17	0.2216	0.0086	0.0385	122.1	91.6	-69.1	-100.6	26.7	3.53
18	0.1093	0.0041	0.0238	55.4	41.6	-30.6	-46.2	26.7	1.64
19	0.0795	0.0030	0.0192	39.1	29.3	-17.7	-34.9	26.7	1.18
20	0.1040	0.0039	0.0229	52.2	39.2	-25.1	-45.8	26.7	1.57
21	0.0600	0.0022	0.0154	27.3	20.5	-10.7	-25.1	26.7	0.82

INTEGRATED FORCES AND MOMENTS FOR THE FULL BIT:

SIERRA WHITE GRANITE AT ROP = 40.0

TOTAL WOB (LBF) = 4830.2

DRILLING TORQ. (FT-LBF) = 700.9

X SIDE FORCE (LBF) = -22.4

Y SIDE FORCE (LBF) = -385.2

RESULTANT SIDE FORCE (LBF) = 385.8

B. M. ABOUT X-AXIS (FT-LBF) = 32.6

B. M. ABOUT Y-AXIS (FT-LBF) = 0.1

Table 9.2 -- Sample output for penetration rate = 40 feet/hour

INTEGRATED AND SUMMARY DATA FOR THE FULL BIT
AT ALL SPECIFIED PENETRATION RATES • :

SIERRA WHITE GRANITE AT ROP =	10.0	20.0	30.0	40.0	50.0
TOTAL WOB (LBF) =	1171.1	2285.8	3517.3	4830.2	6224.4
DRILLING TORQ. (FT-LBF) =	158.1	328.4	511.4	700.9	898.4
X SIDE FORCE (LBF) =	1.4	-5.8	-11.0	-22.4	-34.7
Y SIDE FORCE (LBF) =	-109.0	-179.6	-275.8	-385.2	-496.5
RESULTANT SIDE FORCE (LBF) =	109.0	179.6	276.0	385.8	497.7
B. M. ABOUT X-AXIS (FT-LBF) =	15.3	21.6	27.2	32.6	36.8
B. M. ABOUT Y-AXIS (FT-LBF) =	-1.2	-3.3	-2.5	0.1	3.3
MAX. WEARFLAT TEMP. (DEG. C)=	26.7	26.7	26.7	26.7	26.7
MAX. WEAR RATIO =	5.64	6.15	6.25	6.22	6.11

• BIT DESIGN DATA FROM FILE BITDES.DAT
CUTTER WEAR CONFIGURATION FROM FILE WEARCF.DAT
OPERATING PARAMETER DATA FROM FILE OPCOND.DAT

1
***** NEW CUTTER WEAR CONFIGURATION *****

OBTAINED BY SPECIFYING HARD-ROCK WEAR MODE
AND NEW WEARFLAT AREA OF 0.0020
FOR CUTTER NUMBER 21

COMPUTED LENGTH OF HOLE SINCE LAST WEAR CONF. = 61.3 FT
TOTAL LENGTH OF HOLE DRILLED SINCE START = 61.3 FT
(USING ABRASIVE WEAR CONSTANT OF 0.6890E-12)

(THIS CONFIGURATION WAS STORED IN DISK FILE WCB002.DAT)

CUTTER	WEARFLAT LENGTH (IN.)	WEARFLAT WIDTH (IN.)	WEARFLAT AREA (IN**2)
1	0.021	0.147	0.0022
2	0.033	0.182	0.0041
3	0.037	0.184	0.0049
4	0.045	0.212	0.0064
5	0.044	0.211	0.0063
6	0.043	0.208	0.0061
7	0.040	0.200	0.0055
8	0.036	0.190	0.0046
9	0.035	0.189	0.0045
10	0.039	0.198	0.0053
11	0.039	0.197	0.0052
12	0.038	0.196	0.0051
13	0.041	0.203	0.0056
14	0.041	0.202	0.0056
15	0.042	0.205	0.0058
16	0.037	0.193	0.0049
17	0.036	0.190	0.0046
18	0.028	0.168	0.0032
19	0.023	0.151	0.0024
20	0.026	0.162	0.0028
21	0.020	0.143	0.0020

Table 9.3 -- Sample integrated output for full bit

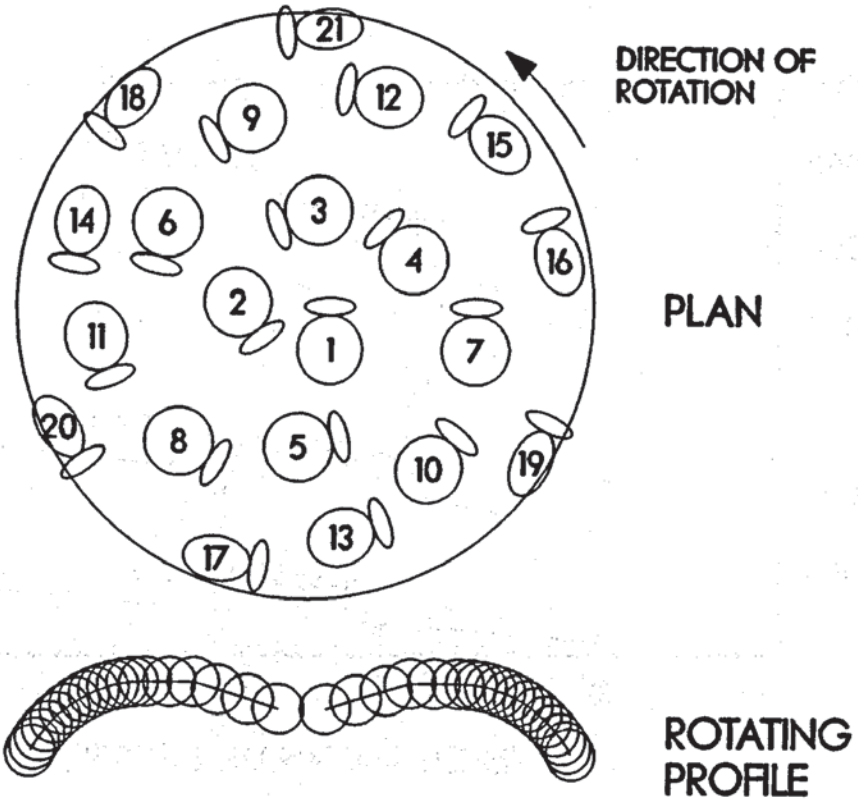

Figure 9.9 -- Bit design used in sample calculation

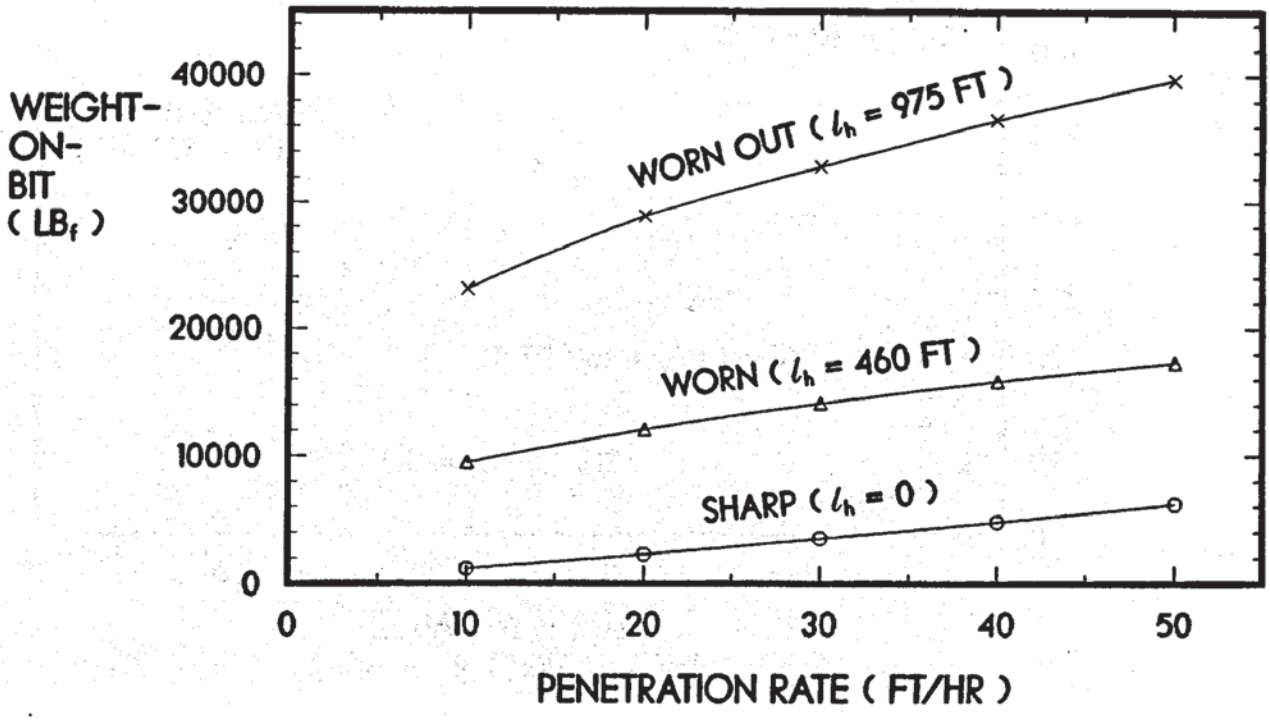

Figure 9.10 -- Predicted weight-on-bit at various penetration rates

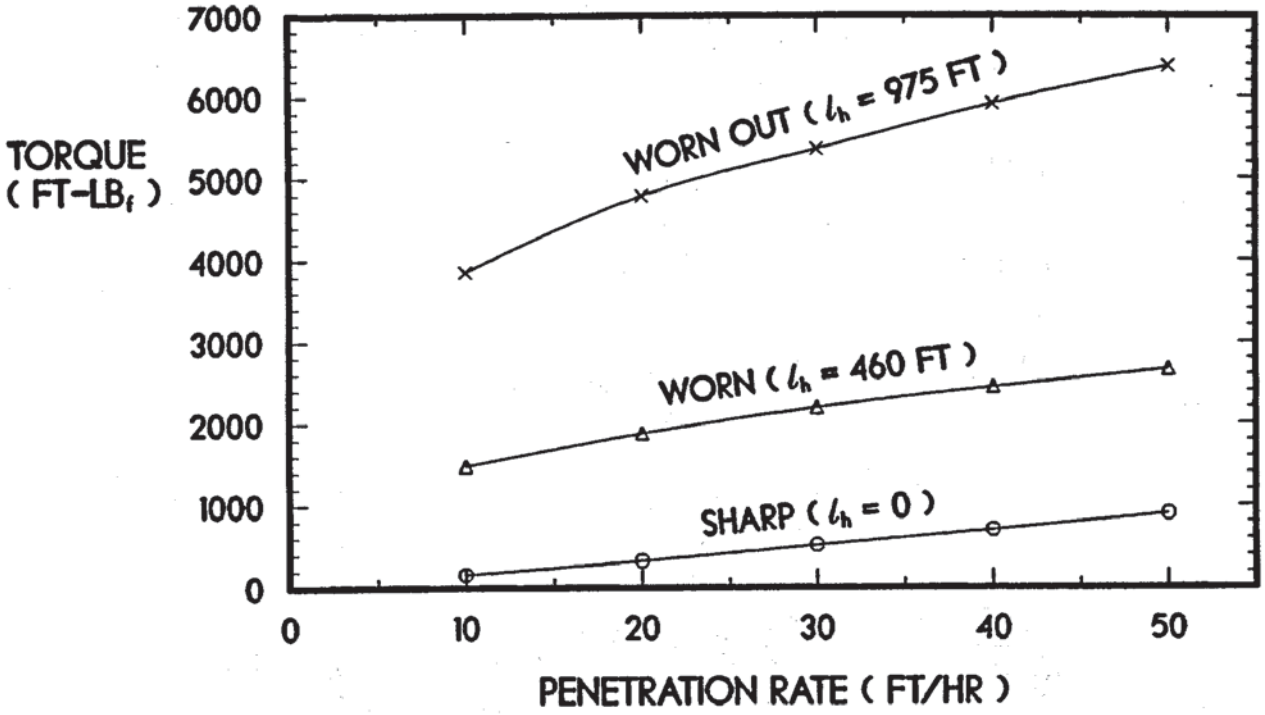

Figure 9.11 -- Predicted torque at various penetration rates

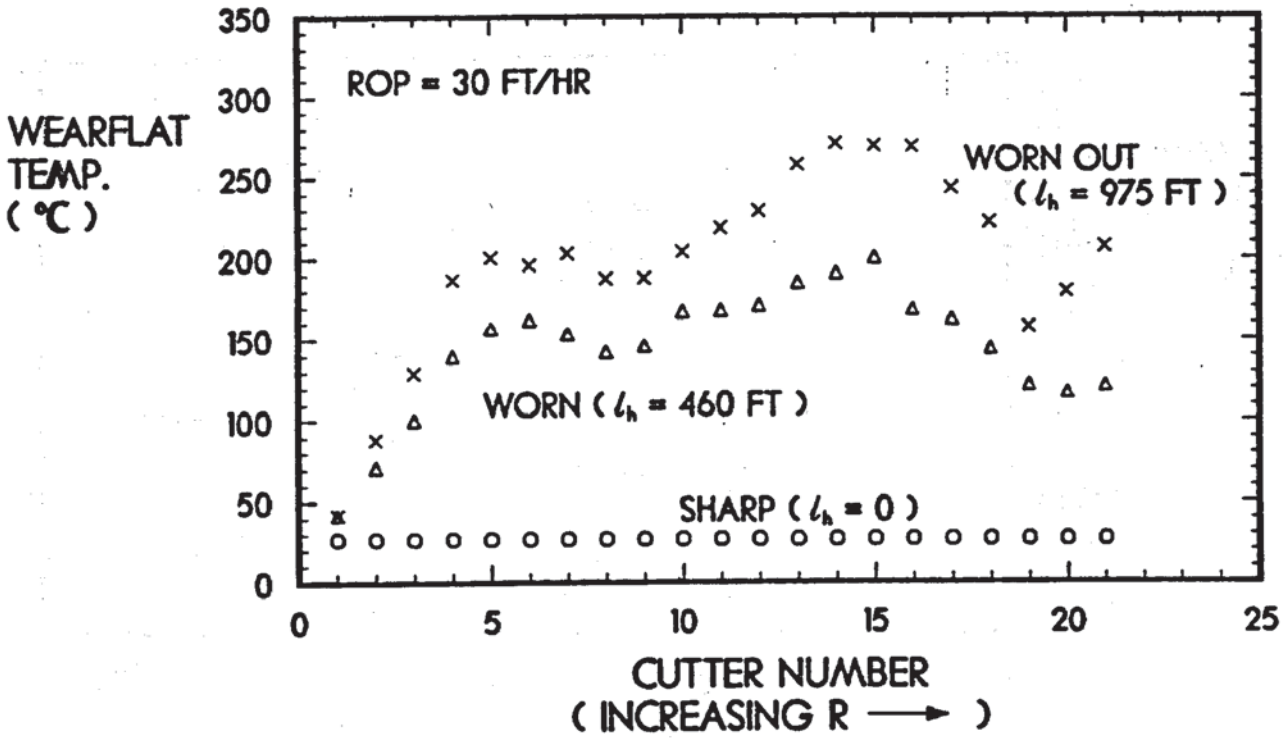

Figure 9.12 -- Predicted cutter wearflat temperatures at progressive stages of bit wear

REFERENCES

1. Pope, L. E., "Analysis of Failed Stratapax^{R}-Steel Stud Cutter Elements," Report SAND80-0410, Sandia Natl. Laboratories, Albuquerque, NM, (April 1981).

2. Huff, C. F., Ashmore, R. F., and Miller, J. W., "Single Point Rock Cutting Strength and Fatigue Evaluation of Gas Pressure Diffusion Bonded Stratapax^{R}," Report SAND77-1962, Sandia Natl. Laboratories, Albuquerque, NM, (April 1978).

3. Jellison, J. L., "Gas Pressure Bonding of Stratapax^{R}," ASME Paper 77-PET-72 presented at Energy Tech. Conf., Houston, TX, Sept. 18-22, 1977.

4. Middleton, J. N. and Finger, J. T., "Diffusion Bonding of Stratapax^{R} for Drill Bits," report SAND82-2309, Sandia Natl. Laboratories, Albuquerque, NM, (January 1983).

5. Huff, C. F., McFall, A. L., and St. Clair, J. A., "Design of Special Performance Bits Utilizing Synthetic Diamond Cutters," paper SPE 7515 presented at the 53rd Annual Fall Tech. Conf. and Exhib. of the Soc. of Petr. Engr., Houston, TX, Oct. 1-4, 1978.

6. Hoover, E. R., and Pope, L. E., "Failure Mechanisms of Polycrystalline Diamond Compact Drill Bits in Geothermal Environments," Report SAND81-1404, Sandia Natl. Laboratories, Albuquerque, NM, (Sept. 1981).

7. Hoover, E. R. and Middleton, J. N., "Laboratory Evaluation of PDC Drill Bits Under High-Speed and High-Wear Conditions," J. Petr. Tech. (Dec. 1981) 2316-2321.

8. Heckes, A. A., Meano, W., and Baker, L. E., "Polycrystalline Diamond Drill Bits for Venezuelan Oil Field Applications," Report SAND82-1963, Sandia Natl. Laboratories, Albuquerque, NM, (April 1983).

9. Swenson, D. V., Wesenberg, D. L., and Jones, A. K., "Analytical and Experimental Investigations of Rock Cutting Using Polycrystalline Diamond Compact Drag Cutter," Paper SPE 10150 presented at the 56th Annual Fall Tech. Conf. and Exhib. of the Soc. of Petr. Engr., San Antonio, TX, (Oct. 5-7, 1981).

10. Zeuch, D. H., Swenson, D. V., and Finger, J. T., "Subsurface Damage Development in Rock During Drag-Bit Cutting: Observations and Model Predictions," Proc. 24th U.S. Symp. on Rock Mech., Texas A&M Univ., College Station, TX, (June 20-23, 1983) 733-742.

11. Swenson, D. V., "Modeling and Analysis of Drag Bit Cutting," Report SAND83-0278, Sandia Natl. Laboratories, Albuquerque, NM, (July 1983).

12. Baird, J. A., Apostal, M. C., Wormley, D. N., "Phase 2 Theoretical Description, A Geological Formation-Drill String Dynamic Interaction Finite Element Program (GEODYN2)," Sandia Natl. Laboratories Contractor Report, SAND86-7084, 1986.

13. Zeuch, D. H. and Finger, J. T., "Rock Breakage Mechanisms with a PDC Bit," Paper SPE 14219 presented at the 60th Annual Tech. Conf. and Exhib. of the Soc. of Petr. Engr., Las Vegas, NV, (Sept. 22-25, 1985).

14. Glowka, D. A., "Optimization of Bit Hydraulic Configurations," Soc. Petr. Engr. J. (Feb. 1983) 21-32.

15. Hibbs, L. E., Jr. and Sogoian, G. C., "Wear Mechanisms for Polycrystalline Diamond Compacts as Utilized for Drilling in Geothermal Environments-Final Report," Report SAND82-7213, Sandia Natl. Laboratories, Albuquerque, NM, (May 1983).

16. Glowka, D. A. and Stone, C. M., "Effects of Thermal and Mechanical Loading on PDC Bit Life," SPE Drilling Engr. (June 1986) 201-214.

17. Ortega, A. and Glowka, D. A., "Studies of the Frictional Heating of Polycrystalline Diamond Compact Tools During Rock Cutting," Report SAND80-2677, Sandia Natl. Laboratories, Albuquerque, NM, (June 1980).

18. Ortega, A. and Glowka, D. A., "Frictional Heating and Convective Cooling of Polycrystalline Diamond Drag Tools During Rock Cutting," Soc. Petr. Engr. J. (April 1984) 121-128.

19. Glowka, D. A. and Stone, C. M., "Thermal Response of Polycrystalline Diamond Compact Cutters Under Simulated Downhole Conditions," Soc. Petr. Engr. J. (April 1984) 143-156.

20. Johnson, V. E., Jr., Lindenmuth, W. T., Chahine, G. L., Conn, A. F., and Frederick, G. S., "Research and Development of Improved Cavitating Jets for Deep-Hole Drilling," Report SAND83-7461, Sandia Natl. Laboratories, Albuquerque, NM, (Jan. 1984).

21. Chahine, G. L., Genoux, P. F., Johnson, V. E., Jr., and Frederick, G. S., "Analytical and Experimental Study of the Acoustics and the Flow Field Characteristics of Cavitating Self-Resonating Water Jets," Report SAND84-7142, Sandia Natl. Laboratories, Albuquerque, NM, (Sept. 1984).

22. Chahine, G. L., Genoux, P. F., Liu, H. L., and Johnson, V. E., Jr., "Analytical and Experimental Study of Self-Resonating Water Jets: Nozzle-Jet and Wall-Jet Interactions," Report SAND84-7142, Sandia Natl. Laboratories, Albuquerque, NM, (July 1987).

23. Chahine, G. L., Johnson, V. E., Jr., Kalumuck, K. M., Perdue, T. O., Waxman, D. N., Frederick, G. S., and Watson, R. E., "Internal and External Acoustics and Large Structures Dynamics of Cavitating

Self-Resonating Water Jets," Report SAND86-7176, Sandia Natl. Laboratories, Albuquerque, NM, (July 1987).

24. Glowka, D. A., "Development of a Method for Predicting the Performance and Wear of PDC Drill Bits", Report SAND86-1745, Sandia Natl. Laboratories, Albuquerque, NM, (Sept. 1987).

25. Glowka, D. A., "The Use of Single-Cutter Data in the Analysis of PDC Bit Designs Paper SPE 15619 presented at the 61st Annual Tech. Conf. & Exhib. of the Soc. of Petroleum Engineers, New Orleans, LA, (October 5-8, 1986).

26. Aronson, E. A., McCaughey, K. G., and Walton, E. L., "STRATAPAX Computer Program Update," Report SAND82-1087, Sandia Natl. Lab., Albuquerque, NM, (Sept. 1982).

APPENDIX A

TEST RESULTS USED TO DETERMINE THE CONSTITUTIVE RELATIONS FOR BEREA SANDSTONE

First character of specimen number refers to coring direction. "Z" direction is normal to bedding planes. "X" and "Y" are mutually orthogonal, but arbitrary.

TABLE 1

UNIAXIAL TEST RESULTS

SPECIMEN	FAILURE STRESS-psi	MODULUS E, x 10^6 psi	POISSON'S RATIO	FAILURE STRAIN, %
X-1-a	7500	1.98	0.20	0.53
X-2-a	7290	1.98	0.33	0.54
X-3-a	7640	2.02	0.65	0.56
X-3-b	7170	1.94	-	0.54
X-4-a	7290	2.01	0.61	0.54
Avg.	7380	1.99	0.45	0.54
Y-1-a	6960	1.74	0.36	0.52
Y-1-b	6810	1.76	0.69	0.49
Y-2-a	7430	1.84	0.24	0.51
Y-2-b	7510	1.87	0.22	0.54
Y-3-a	7520	1.93	0.50	0.55
Avg.	7250	1.82	0.40	0.52
Z-8-a	10190	2.26	0.22	0.68
Z-9-a	9440	2.17	0.23	0.70
Z-9-b	8970	2.09	0.30	0.76
Z-10-a	9310	2.22	0.11	0.64
Z-10-b	9850	2.33	0.29	0.63
Avg.	9550	2.21	0.23	0.68

TABLE 2

TRIAXIAL TEST RESULTS

SPECIMEN	σ_3 psi	FAILURE STRESS-psi	YOUNG'S MODULUS x 10^6 psi	POISSON'S RATIO	FAILURE STRAIN, %
Z-7-a	2000	23890	2.69	0.27	1.35
Z-7-b	2000	23190	2.73	0.24	1.30
Z-8-b	2000	23210	2.54	0.28	1.28
Avg.		23430	2.65	0.26	1.31
Z-1-b	4000	32390	3.37	0.21	1.54
Z-5-b	4000	31350	3.06	0.21	1.63
Z-6-a	4000	32430	3.04	0.23	1.53
Avg.		32060	3.16	0.22	1.57
Z-1-a	6000	38850	2.71	0.10	1.73
Z-2-b	6000	38990	3.05	0.21	1.92
Z-3-b	6000	38130	2.92	0.22	1.77
Avg.		38660	2.89	0.18	1.81
Z-3-a	7500	43140	2.74	0.10	1.96
Z-4-a	7500	42920	3.17	0.20	1.91
Z-4-b	7500	43540	3.08	0.21	1.97
Avg.		43200	2.99	0.17	1.95

TABLE 3

TENSILE TEST RESULTS

SPECIMEN	DIAM. inch	LENGTH inch	FAILURE LOAD-lbs.	FAILURE STRESS-psi
X-1-b	2.140	1.062	1440	403
X-1-c	2.141	1.017	1185	346
X-1-d	2.140	.963	1265	391
X-2-b	2.140	1.052	1235	349
X-2-c	2.140	1.013	1140	335
X-2-d	2.139	1.056	1232.5	347
			Avg.	362
Y-1-c	2.140	1.028	1402.5	406
Y-1-d	2.140	.958	1012.5	314
Y-2-c	2.140	1.018	1165	340
Y-2-d	2.140	.995	1135	339
Y-3-c	2.141	1.038	1265	362
Y-3-d	2.141	1.026	1560	452
			Avg.	369
Z-1-c	2.143	1.033	1422.5	409
Z-1-d	2.143	1.021	1467.5	427
Z-2-c	2.141	1.022	1315	383
Z-2-d	2.141	1.007	1747.5	516
Z-3-c	2.142	.996	1172.5	350
Z-3-d	2.142	1.025	1397.5	405
			Avg.	415

TABLE 4

MEASURED FRACTURE ANGLES

SPECIMEN	σ_3 psi	β	Avg. β	ϕ
X-1-a	0	70°		
X-2-a		74°		
X-3-a		71°		
X-3-b		68°		
X-4-a		75°	71.6°	53.2°
Y-1-a	0	71°		
Y-1-b		64°		
Y-2-a		66°		
Y-2-b		73°		
Y-3-a		65°	67.8°	45.6°
Z-8-a	0	72°		
Z-9-a		73°		
Z-9-b		66°		
Z-10-a		74°		
Z-10-b		74°	71.8°	53.6°
Z-7-a	2000	70°		
Z-7-b		n.a.		
Z-8-b		67°	68.5°	47.°

TABLE 4 (cont.)

MEASURED FRACTURED ANGLES

SPECIMEN	σ_3 psi	β	Avg. β	ϕ
Z-1-b	4000	n.a.		
Z-5-b		71°		
Z-6-a		66°	68.5°	47.°
Z-1-a	6000	54°		
Z-2-b		58°		
Z-3-b		58°	56.7°	23.4°
Z-3-a	7500	60°		
Z-4-a		58°		
Z-4-b		62°	60.°	30.°

The angle, β, between a plane normal to the core axis and the fracture plane was measured for each specimen at the end of the test. These angles, as well as the average values for uniaxial tests in each direction, and triaxial tests at each level of confining pressure are presented in Table 4. If the Coulomb failure criterion is assumed, the angle of internal friction can be calculated by:

$$\phi = 2(\beta - 45^\circ)$$

DISTRIBUTION:
DOE/TIC-4500-UC-253 (10)

Dr. J. J. Azar
Tulsa University Drilling
Research Projects
Petroleum Engineering Dept.
North Campus Drill Bldg.
2450 Marshall
Tulsa, OK 74110

Bill Baker
Smith Tool
P. O. Box C-19511
Irvine, CA 92713

Ed Bingman
Shell Oil Co.
Two Shell Plaza
P. O. Box 2099
Houston, TX 77001

Alan Black
Drilling Research Laboratory
University Research Park
400 Wakara Way
Salt Lake City, UT 84108

Gerald R. Boyle
Anco Diamond Composite Corp.
545 Fifth Ave.
New York, NY 10017

Ben Bradford
Dowell
P. O. Box 2710
Tulsa, OK 74102

John Cheatham
Rice University
Mechanical Engineering Dept.
P. O. Box 1892
Houston, TX 77001

David Clark
Conoco Production Research
P. O. Box 1267
Ponca City, OK 74603

Jim Combs
Geothermal Resourches Int'l., Inc.
1825 W. Grant, Suite 900
San Mateo, CA 94402

Brett Davies
Huddy International
Suite 304
7061 S. University Blvd.
Littleton, CO 80122

Dr. Melvin Friedman
Center for Technophysics
and Dept. of Geology
College Station, TX 77843

Daniel Garcia
Tulsa University Drilling
Research Projects
Petroleum Engineering Dept.
North Campus Drill Bldg.
2450 Marshall
Tulsa, OK 74110

Louis Hibbs, Jr.
General Electric Co.
P. O. Box 8, Bldg. K-1
Schenectady, NY 12301

Dr. Michael Hood
University of California
Dept. of Materials Science &
Minerals Engineering
Berkeley, CA 94720

James Langford
Security Division
Dresser Industries
P. O. Box 2467
Dallas, TX 75224

B. J. Livesay
Livesay Consultants
2613 Angell Ave.
San Diego, CA 92122

Ed Martin
Mobil Research &
Development Corporation
Dallas Research Laboratory
13777 Midway Rd.
Dallas, TX 75224

Larry Matson
Stratabit
600 Kenrick, Suite A1
Houston, TX 77060

William Maurer
Maurer Engineering, Inc.
10301 NW Freeway
Suite 202
Houston, TX 77205

Keith Millheim
Amoco Production Company
Research Center
P. O. Box 591
Tulsa, OK 74102

Alfonso Ortega
Dept. of Aerospace &
Mechanical Engineering
College of Engineering & Mines
University of Arizona
Tucson, Arizona 85721

Gene Polk
P. O. Box 280
Sandia Park, NM 87047

Steve Pye
Union Geothermal Division
Union Oil Co. of California
Union Oil Center
461 S. Boylston
Los Angeles, CA 90017

Troy Reed
Conoco Production Research
P. O. Box 1267
Ponca City, OK 74603

Jim Riechman
FlowDril Corporation
21414 - 68th Ave. S.
Kent, WA 98032

John C. Rowley
Los Alamos National Laboratory
Mail Stop 462
Los Alamos, NM 87545

U.S. Dept. of Energy (2)
Geothermal Technologies Div.
Attn: Lew Pratsch
Marshall Reed
Forrestal Bldg., CE-324
1000 Independence Ave., SW
Washington, DC 20585

George P. Tennyson
DOE/ALO
P. O. Box 5400
Albuquerque, NM 87115

Sam Varnado
Titan-Spectron
2017 Yale Blvd., SE
Albuquerque, NM 87106

Bruce Walker
Drilling Research Laboratory
University Research Park
400 Wakara Way
Salt Lake City, UT 84108

Tom Warren
Amoco Production Company
Research Center
P. O. Box 591
Tulsa, OK 74102

John Barr
NL Hycalog
Oldends Lane
Industrial Estate
Stonehouse, Gloucester
England GL10 3RQ

Rubin Feenstra
Shell Research B.V.
Volmerlaan 6
2288 GD Rijswijk ZH
The Netherlands

3141	S. A. Landenberger (5)
3151	W. I. Klein (3)
3154-1	C. L. Ward for DOE/OSTI (8)
5260	J. R. Kelsey
6200	V. L. Dugan
6250	R. K. Traeger
6252	J. C. Dunn (5)
6252	J. T. Finger (20)
6252	D. A. Glowka (10)
6252	P. C. Lysne
6314	T. E. Hinkebein
8524	J. R. Wackerly